Using nickel to fold discrete synthetic macromolecules into single-chain nanoparticles

Melissa A. Reith,[a] Sinan Kardas,[b,c] Chiel Mertens,[a] Mathieu Fosséprè,[b] Mathieu Surin,[b]* Jan Steinkoenig,[a]* Filip E. Du Prez[a]*

Supporting Information

Table of Content

a *M.A. Reith, C. Mertens, J. Steinkoenig, F.E. Du Prez*
Polymer Chemistry Research Group
Centre of Macromolecular Chemistry (CMaC)
Department of Organic and Macromolecular Chemistry
Faculty of Sciences
Ghent University
Krijgslaan 281 S4-bis, Ghent B-9000
Belgium
Email: Filip.DuPrez@ugent.be, Jan.Steinkonig@ugent.be
b *S. Kardas, Dr. M. Fosséprè, Dr. M. Surin*
Laboratory for Chemistry of Novel Materials
Center of Innovation and Research in Materials and Polymers
University of Mons
Place du Parc 20, Mons B-7000
Belgium
E-mail: Mathieu.Surin@umons.ac.be
c *S. Kardas*
Institute for Complex Molecular Systems
Eindhoven University of Technology
P.O. Box 513, Eindhoven 5600 MB
The Netherlands

Experimental

Materials

The reagents were purchased from commercial suppliers and unless otherwise stated used as supplied.

Characterization

Liquid chromatography mass spectroscopy (LC-MS).

LC-MS spectra were recorded on an Agilent technologies 1100 series LC/MSD system equipped with a diode array detector and single quad MS detector (VL) with an electrospray source (ESI-MS) for classic reversed phase LCMS and MS analysis. All results were recorded in positive mode unless otherwise stated. Analytic reversed phase HPLC (high-performance liquid chromatography) was performed with a Phenomenex C18 (2) column (5 µ, 250 × 4.6 mm) using a solvent gradient (0 → 100 % acetonitrile in H_2O in 15 min) and the eluting compounds were detected via UV-detection (λ = 254 nm).

Nuclear magnetic resonance (NMR) spectroscopy.

^1H spectra were recorded on a Bruker Avance 300 (300 MHz), a Bruker Avance 400 (400 MHz) or a Bruker Avance II 500 (500 MHz) and DOSY spectra were recorded at 500 MHz on a Bruker Avance 500. Methanol-d_4 (CD_3OD), DMSO-d_6 or DMF-d_7 were used as solvents. Chemical shifts are presented in parts per million (δ) and calibrated to the characteristic residual solvent signal at 2.50 ppm (^1H, DMSO-d_6), 3.31 ppm (^1H, CD_3OD) and 49.00 ppm (^{13}C, CD_3COD), or 1.94 ppm (^1H, DMF-d_7).

Ultraviolet–visible (UV-Vis) spectroscopy.

UV-Vis spectra were recorded on an Analytik Jena Specord200 in methanol.

High resolution electrospray ionization mass spectrometry (ESI-MS).

Mass spectra were recorded on a Q Excative (Orbitrap) mass spectrometer (Thermo Fisher Scientific, San Jose, CA, USA) equipped with an atmospheric pressure ionization source operating in the nebulizer assisted electrospray mode. The instrument was calibrated in the m/z-range 150-2000 using a standard containing caffeine, Met-Arg-Phe-Ala acetate (MRFA) and a mixture of fluorinated phosphazenes (Ultramark 1621, all from Sigma Aldrich). A constant spray voltage of 3.5 kV, a dimensionless sheath gas of 6, and a sweep gas flow rate of 2 were applied. The capillary voltage and the S-lens RF level were set to 68.0 V and 320°C, respectively.

Liquid handling robot

Automated solid-phase synthesis was performed on a peptide synthesiser INTAVIS MultiPep RSI, equipped with a vortexing unit and a 72-reactor block with open 5 mL PE reactor columns. The speed of the vortexing was 700 rpm.

Synthesis

Chiral resolution of DL-homocysteine thiolactone hydrochloride (TLa-NH_2.HCl) to obtain enantiomeric enriched D-homocysteine thiolactone hydrochloride[1,2]

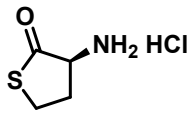

DL-homocysteine thiolactone hydrochloride (TLa-NH_2.HCl) (500 g, 3.25 mol, 1.00 eq.) was suspended in technical acetone (2.5 L) using a mechanical stirrer. After the slow addition of triethylamine (453 mL, 3.25 mol, 1.00 eq.), the mixture was stirred for two hours. The formed triethylamine hydrochloride salt was filtered, the residue was washed with acetone (3 x 200 mL) and the filtrates were combined. Successively *(R)*-mandelic acid (495 g, 3.25 mol, 1.00 eq.) and salicylaldehyde (50 mL, 0.47 mol, 0.15 eq.) were added under mechanical stirring. The suspension was stirred for 18 hours. The rapidly formed diastereomeric salt was collected by filtration and then washed with acetone (5 x 300 mL). After suspending the residue in acetone (5 L), concentrated aqueous hydrochloric acid solution (250 mL, 2.5 mol) was slowly added and stirred with a mechanical stirrer overnight. The solid was filtered off, washed with acetone (3 x 200 mL) and dried in a vacuum oven at 40 °C yielding *(R)*-homocysteine thiolactone hydrochloride as a white solid. Yield: 291.6 g. 1.898 mol, 59%, 97.9%ee.

Synthesis of 5-oxo-5-((2-oxotetrahydrothiophen-3-yl)amino)pentanoic acid (TLa-COOH)[3]

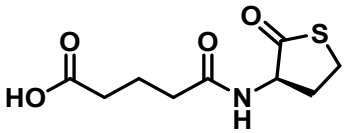

(R)-TLa NH_2.HCl (30.0 g, 0.20 mol, 1.00 eq.) was dissolved in 450 mL H_2O/1,4-dioxane mixture (ratio 1:1) and cooled with an ice bath. Sodium bicarbonate (82.0 g, 0.98 mol, 5.00 eq.) were added portion wise. The reaction mixture was stirred for 30 min. Then glutaric anhydride (44.6 g, 0.39 mol, 2.00 eq.) was slowly added. The mixture was allowed to warm up to room temperature and stirred overnight. By the addition of concentrated aqueous hydrochloric acid solution, the pH of the solution was adjusted to 1. The white precipitate was filtered off and dried. The solution was extracted with ethyl acetate (3 x 200 mL). The combined organic phases were dried using magnesium sulphate, filtered and the solvent was removed under reduced pressure. The remaining solid was recrystallized in acetone. TLa-COOH was obtained as white crystals after filtration. Yield: 41.7 g, 0.18 mol, 93%.

Synthesis of oligomers

Loading of resin

2-chlorotrityl chloride resin (3.00 g, 1.60 mmol/g) was loaded with TLa-COOH (1.66 g, 1.50 eq. relative to resin) in a mixture of 30 mL dry DCM, 3 mL dry DMF and 5 mL dry N,N-diisopropylethylamine (DIPEA). The reactor was sealed with a rubber septum and put under argon conditions. The reaction mixture was shaken for 3 hours. The resin was washed with a DCM/MeOH/DIPEA (17:2:1, 3 x 30 mL) mixture, DCM (3 x 30 mL), DMF (2 x 30 mL), DCM (2 x 30 mL) and diethyl ether (3 x 30 mL) and dried under reduced pressure. The loading was determined to be 1.0 mmol/g via a literature procedure.[4]

General Procedure for aminolysis and functionalization with 2-(chloromethyl)pyridine hydrochloride

DMF was added to the loaded resin (1 mL per 100 mg of solid support). The mixture was shaken for 10 min to allow swelling of the resin. Then dithiolthreitol (DTT, 1 eq.), water and ethanolamine (50 eq.) were added. The reaction mixture was shaken for 15 min. In the next step, 2-(chloromethyl)pyridine hydrochloride (30 eq.) and potassium iodide (50 eq.) were added and the mixture was shaken for 30 min. The reaction solution was filtered off and the solid support was washed twice with water and DMF. Then the procedure was repeated to ensure the full conversion. After the repetition, the resin was washed with DMF (4x), methanol (4x), $CHCl_3$ (4x) and diethyl ether (4x) and dried.

General Procedure for aminolysis and functionalization with methyl acrylate

The solid support was swollen for 10 min in $CHCl_3$ (1 mL per 100 mg of resin). Methyl acrylate (20 eq.) and ethanolamine (10 eq.) were added successively. The reaction mixture was shaken for 15 min. The solution phase was filtered off and the procedure was repeated a second time to ensure complete conversion. Then, the solid phase was washed with DMF (4x), methanol (4x), $CHCl_3$ (4x) and diethyl ether (4x) and dried.

General Procedure for the elongation with TLa-COOH

The resin was swollen in DMF (1 mL per 100 mg of solid support) for 10 min. Successively, TLa-COOH (10.9 eq.), *N,N'*-diisopropylcarbodiimide (DIC, 10 eq.) and 4-dimethylaminopyridine (DMAP, 0.5 eq.) were added. After 1 hour of shaking, the reaction mixture was filtered off and the addition step was repeated. The resin was washed with DMF (4x), methanol (4x), $CHCl_3$ (4x), diethyl ether (4x).

General Procedure for the automated protocol using the peptide synthesizer

Stock solutions for the reagents were prepared as followed:

- Solution 1: ethanolamine (3 mol/L) in chloroform
- Solution 2: methyl acrylate (3 mol/L) in chloroform
- Solution 3: 5-oxo-5-((2-oxotetrahydrothiophen-3-yl)amino)pentanoic acid (*(R)*-TLa-COOH) (0.7 mol/L) in dimethylformamide
- Solution 4: 4-dimethylaminopyridine (DMAP) (0.4 mol/L) in dimethylformamide
- Solution 5: *N,N'*-diisopropylcarbodiimide (DIC) (3.2 mol/L) in dimethylformamide

For the washing steps, dimethylformamide was taken from a 2.5 L solvent bottle by the machine, chloroform and methanol were added separately. The current protocol was adapted from a published method.[2]

100 mg of thiolactone-functionalised 2-chlorotrityl chlorine resin with a loading of 1.0 mmol/g was used for the automated synthesis. For the aminolysis and functionalisation with methyl acrylate 1333.33 µL of the methyl acrylate solution was taken (40.00 eq.). Next, 666.67 µL of the ethanolamine solution was taken (20.00 eq.). For the chain extension 1540.00 µL of the *(R)*-TLa-COOH solution was added (10.78 eq.). Followed by the addition of 312.50 µL of DIC solution (10.00 eq.) and 250.00 µL of the DMAP solution (1.00 eq.).

Compaction with Ni(II) ions

The sequence (1.0 eq.) was dissolved in methanol-d_4 (0.01-0.02 mol/L) in an NMR-tube. Nickel(II)perchlorate (1.0 eq.) was added and the reaction was shaken for 24 hours to give Ni(II)-SD-SCNP.

Compaction with Cu(II) ions

In an NMR-tube, a sequence was dissolved in methanol-d_4 (0.003 mol/L). Copper(II)perchlorate (1 eq.) was added and the reaction mixture was shaken for 5 hours. After the addition of sodium chloride (1.0 eq.), the mixture was shaken for one hour.

LC-MS traces of sequence-defined oligomers

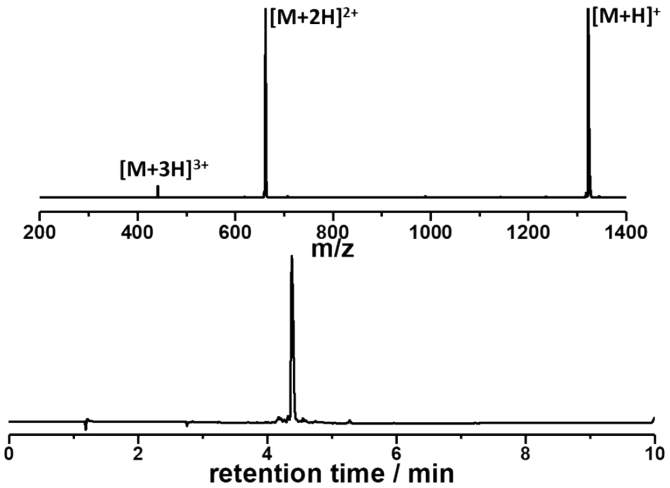

Figure S1. LC-MS trace of trimer consisting of two picolyl moieties and one methyl acrylate unit.

Table S1. Assignment of the peak of the trimer (Figure 1).

Abbreviation	Structure	Sum Formula	m/z (exp)	m/z (theo)	Δm/z
$[M+H]^+$	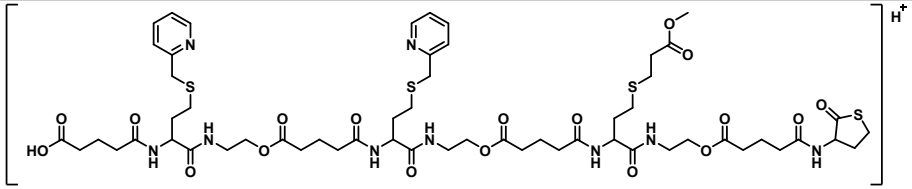	$C_{58}H_{84}N_9O_{18}S_4$	1322.308	1322.4812	0.173
$[M+2H]^{2+}$	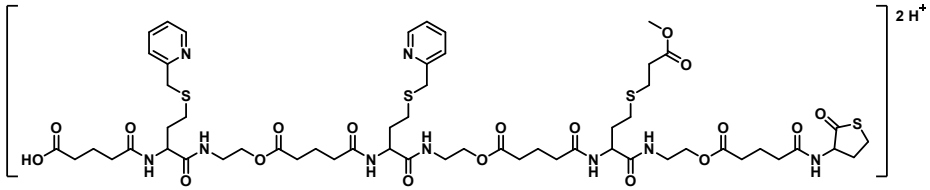	$C_{58}H_{85}N_9O_{18}S_4$	661.873	661.744	0.129
$[M+3H]3^+$	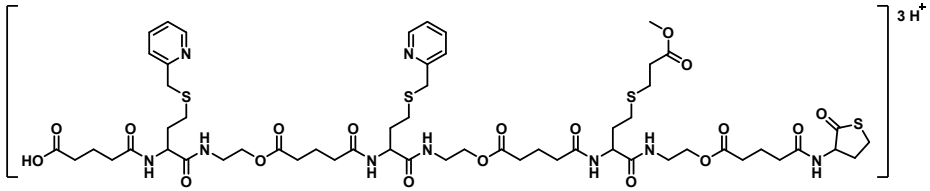	$C_{58}H_{86}N_9O_{18}S_4$	441.723	441.500	0.223

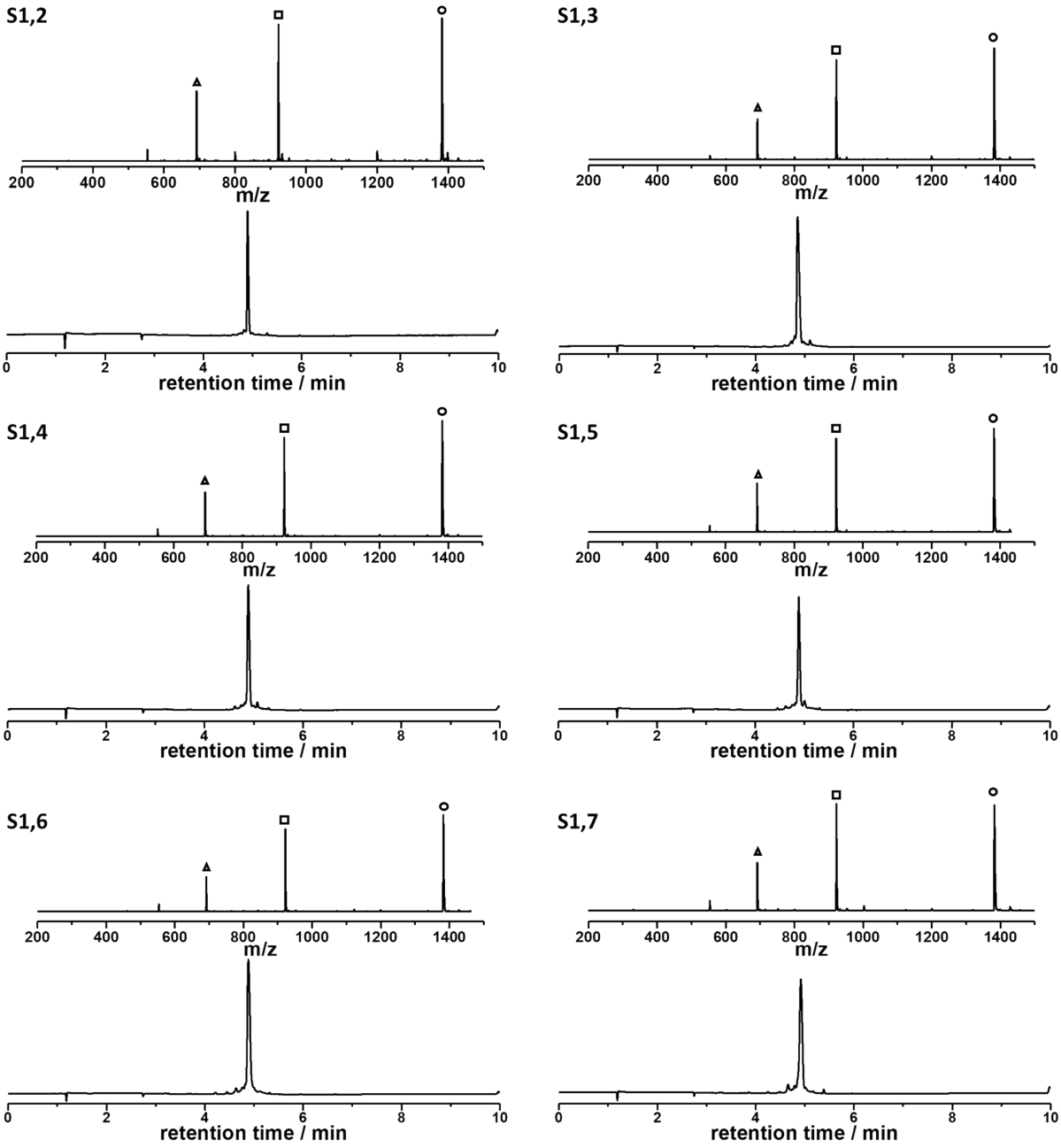

Figure S2. LC ESI-MS traces of the heptamers with various spacer units in between two picolyl functionalities. ▯ double charged □ triple charged Δ quadruple charged mass of the heptamer.

Table S2. Assignment of the peaks of sequence S1,2 (Figure S2).

Abbreviation	Structure	Sum Formula	m/z (exp)	m/z (theo)	Δm/z
□	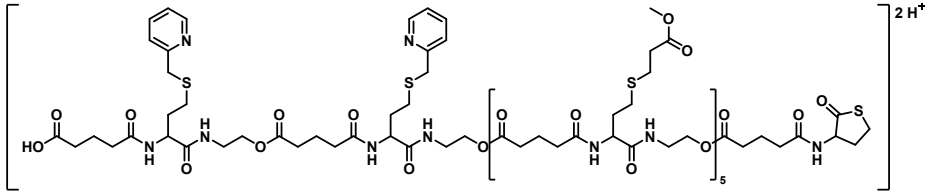	$C_{118}H_{181}N_{17}O_{42}S_8$	1381.757	1382.015	0.445
□	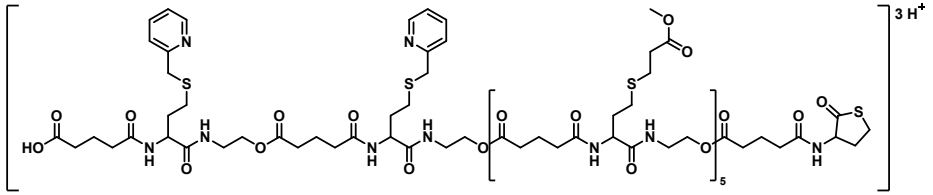	$C_{118}H_{182}N_{17}O_{42}S_8$	921.531	921.679	0.148
Δ	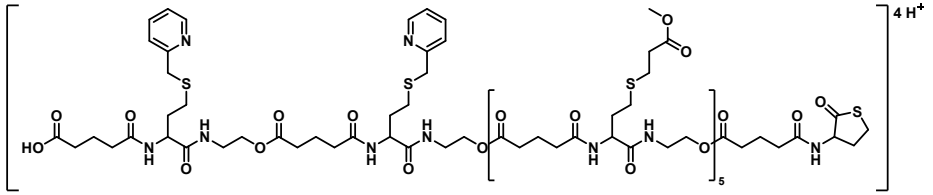	$C_{118}H_{183}N_{17}O_{42}S_8$	691.429	691.511	0.082

Table S3. Assignment of the peaks of sequence S1,3 (Figure S2).

Abbreviation	Structure	Sum Formula	m/z (exp)	m/z (theo)	Δm/z
□	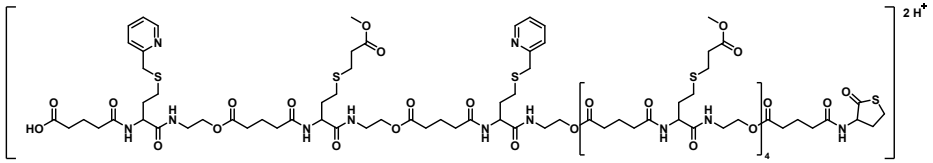	$C_{118}H_{181}N_{17}O_{42}S_8$	1381.731	1382.015	0.284
□	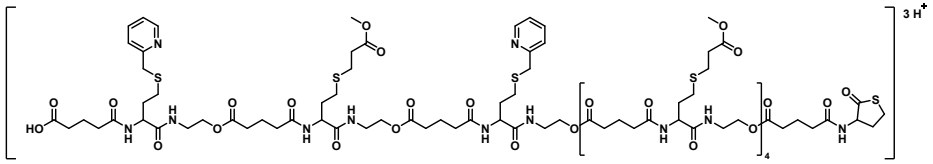	$C_{118}H_{182}N_{17}O_{42}S_8$	921.410	921.679	0.269
Δ	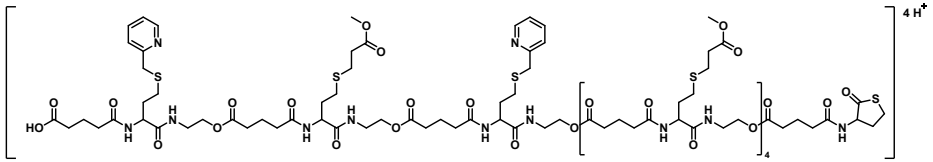	$C_{118}H_{183}N_{17}O_{42}S_8$	691.308	691.511	0.203

Table S4. Assignment of the peaks of sequence S1,4 (Figure S2).

Abbreviation	Structure	Sum Formula	m/z (exp)	m/z (theo)	Δm/z
□	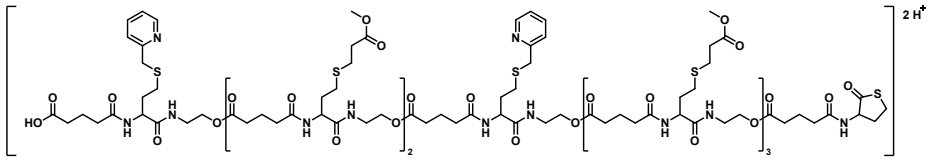	$C_{118}H_{181}N_{17}O_{42}S_8$	1381.875	1382.015	0.140
□	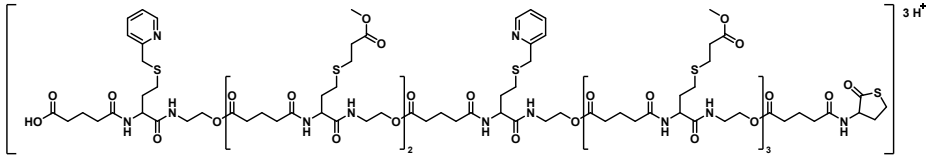	$C_{118}H_{182}N_{17}O_{42}S_8$	922.111	921.679	0.432
Δ	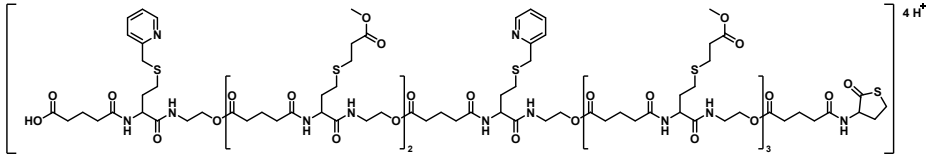	$C_{118}H_{183}N_{17}O_{42}S_8$	691.880	691.511	0.369

Table S5. Assignment of the peaks of sequence S1,5 (Figure S2).

Abbreviation	Structure	Sum Formula	m/z (exp)	m/z (theo)	Δm/z
□	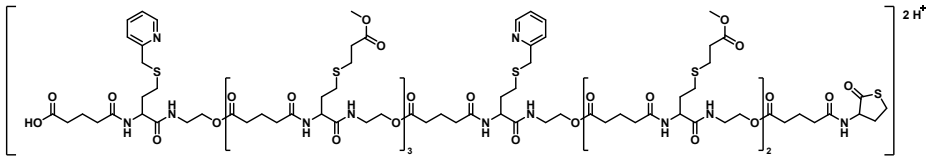	$C_{118}H_{181}N_{17}O_{42}S_8$	1381.731	1382.015	0.284
□	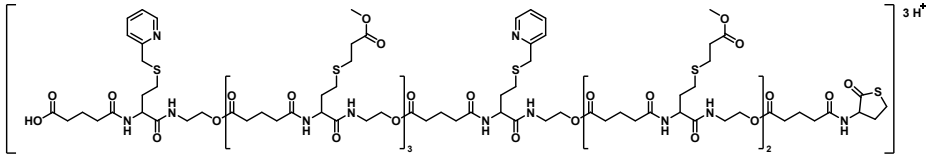	$C_{118}H_{182}N_{17}O_{42}S_8$	921.523	921.679	0.156
Δ	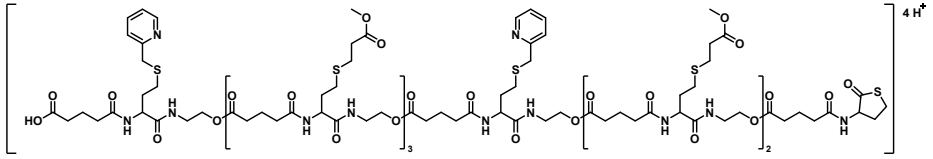	$C_{118}H_{183}N_{17}O_{42}S_8$	691.644	691.511	0.133

Table S6. Assignment of the peaks of sequence S1,6 (Figure S2).

Abbreviation	Structure	Sum Formula	m/z (exp)	m/z (theo)	Δm/z
□	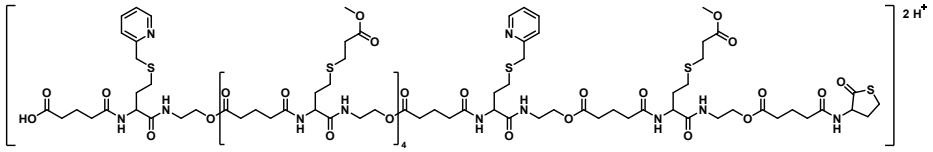	$C_{118}H_{181}N_{17}O_{42}S_8$	1381.806	1382.015	0.209
□	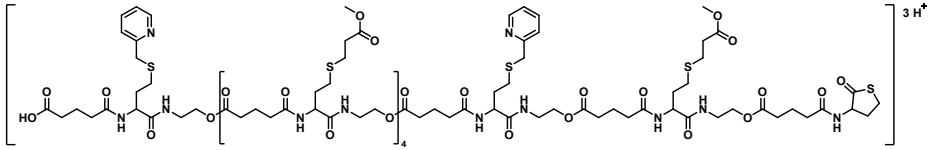	$C_{118}H_{182}N_{17}O_{42}S_8$	922.058	921.679	0.379
Δ	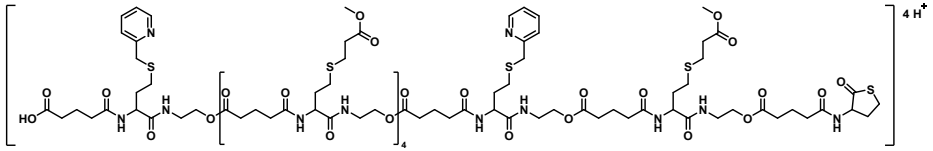	$C_{118}H_{183}N_{17}O_{42}S_8$	691.871	691.511	0.360

Table S7. Assignment of the peaks of sequence S1,7 (Figure S2).

Abbreviation	Structure	Sum Formula	m/z (exp)	m/z (theo)	Δm/z
□	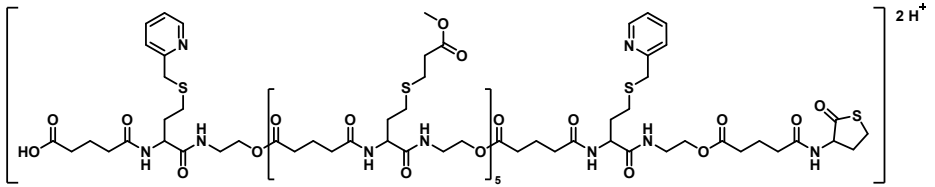	$C_{118}H_{181}N_{17}O_{42}S_8$	1381.880	1382.015	0.135
□	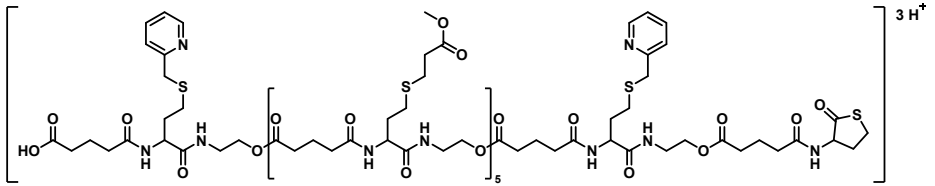	$C_{118}H_{182}N_{17}O_{42}S_8$	921.923	921.679	0.244
Δ	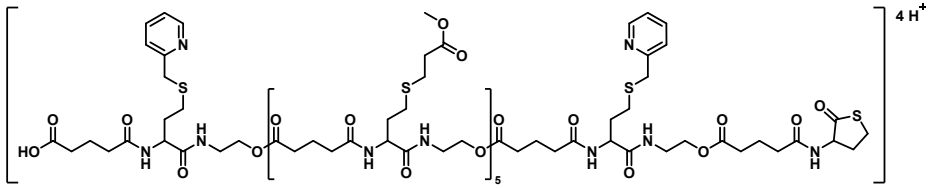	$C_{118}H_{183}N_{17}O_{42}S_8$	691.837	691.511	0.326

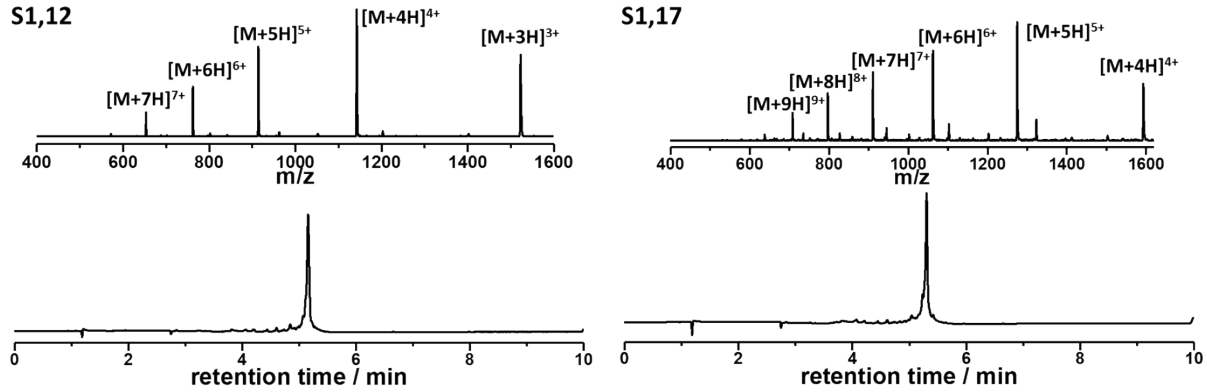

Figure S3. LC ESI-MS traces of the dodecamer S1,12 and the heptadecamer S1,17.

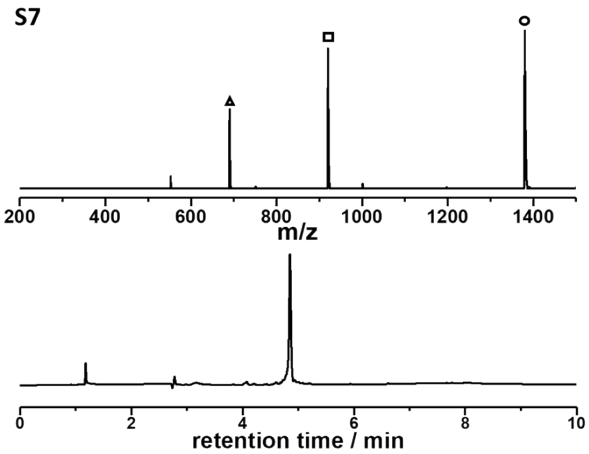

Figure S4. LC ESI-MS trace of reference heptamer S7, containing one picolyl functionality.
 double charged □ triple charged Δ quadruple charged mass of the heptamer.

Table S8. Assignment of the peaks of sequence S1,12 (Figure S3).

Abbreviation	Structure	Sum Formula	m/z (exp)	m/z (theo)	Δm/z
$[M+3H]^{3+}$	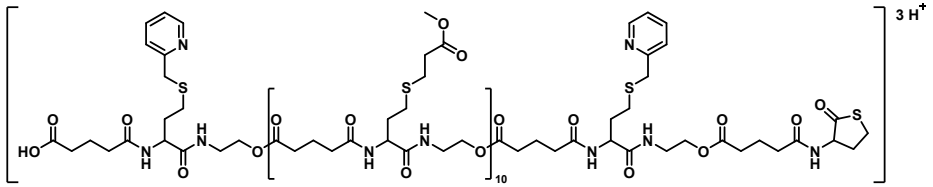	$C_{193}H_{302}N_{27}O_{72}S_{13}$	1521.924	1521.905	0.019
$[M+4H]^{4+}$	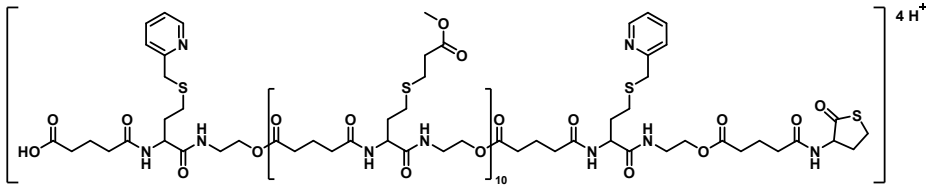	$C_{193}H_{303}N_{27}O_{72}S_{13}$	1141.709	1141.681	0.028
$[M+5H]^{5+}$	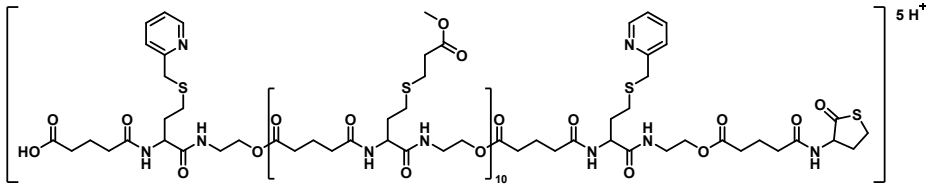	$C_{193}H_{304}N_{27}O_{72}S_{13}$	913.466	913.546	0.080
$[M+6H]^{6+}$	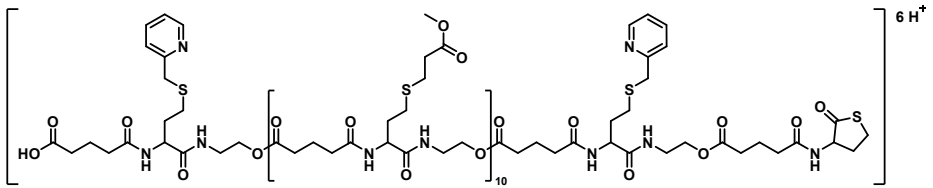	$C_{193}H_{305}N_{27}O_{72}S_{13}$	761.378	761.456	0.078
$[M+7H]^{7+}$	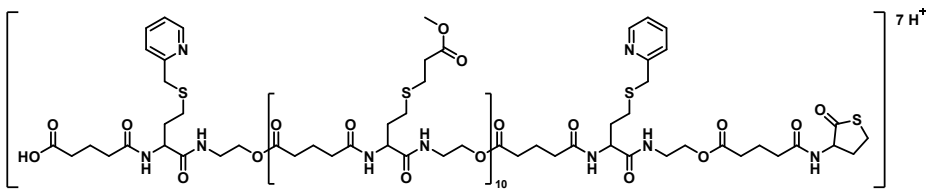	$C_{193}H_{306}N_{27}O_{72}S_{13}$	653.226	652.821	0.405

Table S9. Assignment of the peaks of sequence S1,17 (Figure S3).

Abbreviation	Structure	Sum Formula	m/z (exp)	m/z (theo)	Δm/z
$[M+4H]^{4+}$	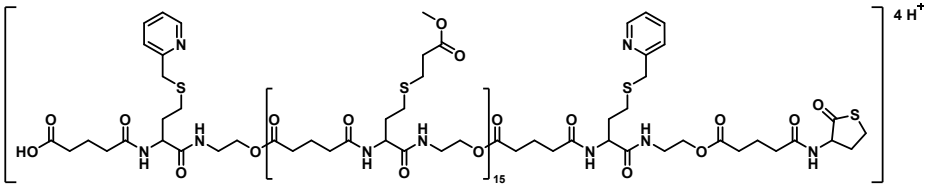	$C_{268}H_{423}N_{37}O_{102}S_{18}$	1591.945	1591.850	0.095
$[M+5H]^{5+}$	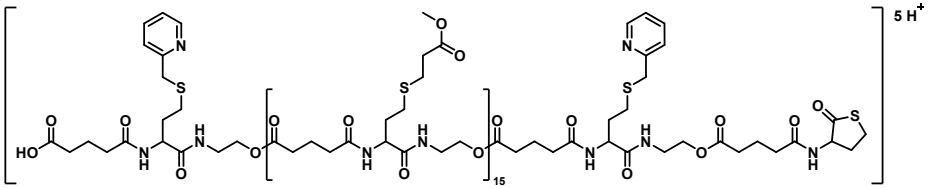	$C_{268}H_{424}N_{37}O_{102}S_{18}$	1273.661	1273.681	0.020
$[M+6H]^{6+}$	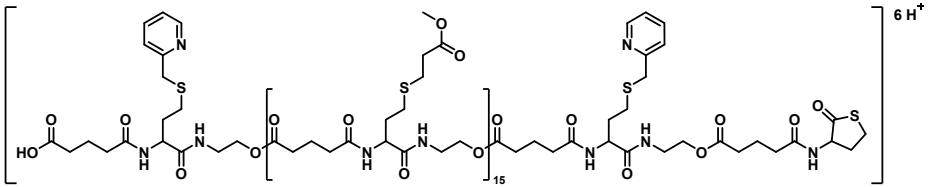	$C_{268}H_{425}N_{37}O_{102}S_{18}$	1061.428	1061.569	0.141
$[M+7H]^{7+}$	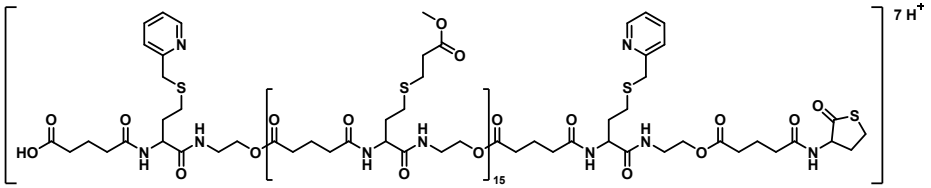	$C_{268}H_{426}N_{37}O_{102}S_{18}$	909.938	910.060	0.122
$[M+8H]^{8+}$	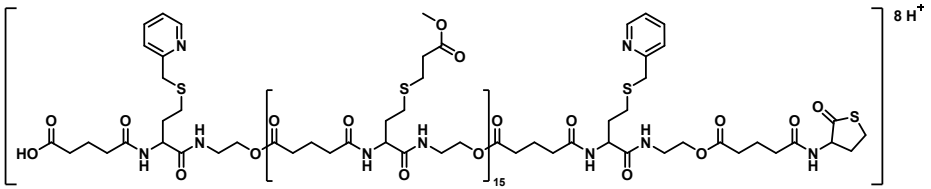	$C_{268}H_{427}N_{37}O_{102}S_{18}$	796.389	796.429	0.04
$[M+9H]^{9+}$	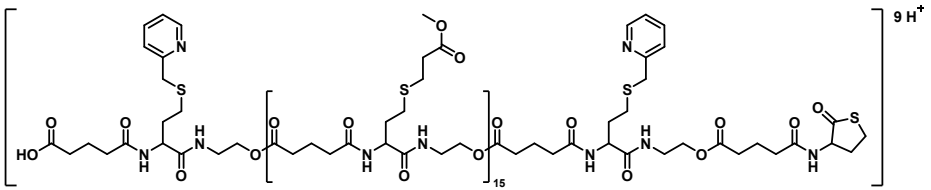	$C_{268}H_{428}N_{37}O_{102}S_{18}$	707.926	708.049	0.123

Table S10. Assignment of the peaks of sequence S7 (Figure S4).

Abbreviation	Structure	Sum Formula	m/z (exp)	m/z (theo)	Δm/z
□	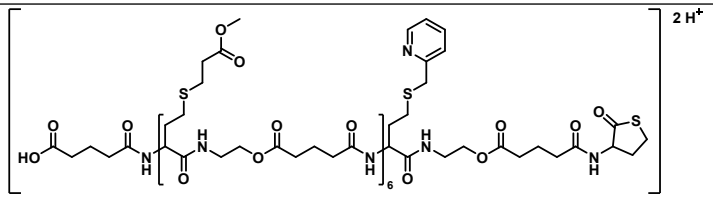	$C_{118}H_{181}N_{17}O_{42}S_8$	1379.813	1379.513	0.300
□	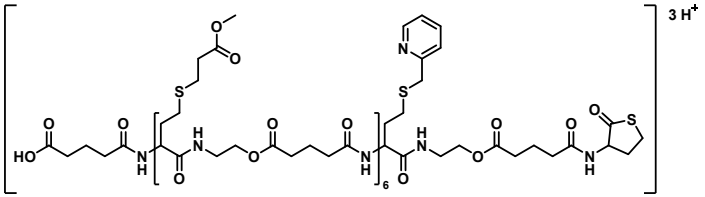	$C_{118}H_{182}N_{17}O_{42}S_8$	920.529	920.011	0.518
Δ	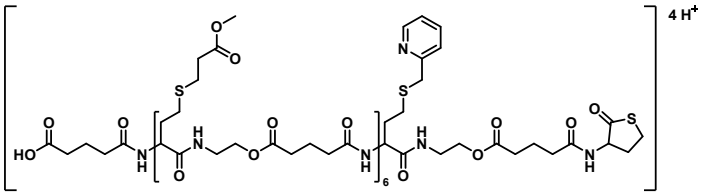	$C_{118}H_{183}N_{17}O_{42}S_8$	690.260	690.646	0.386

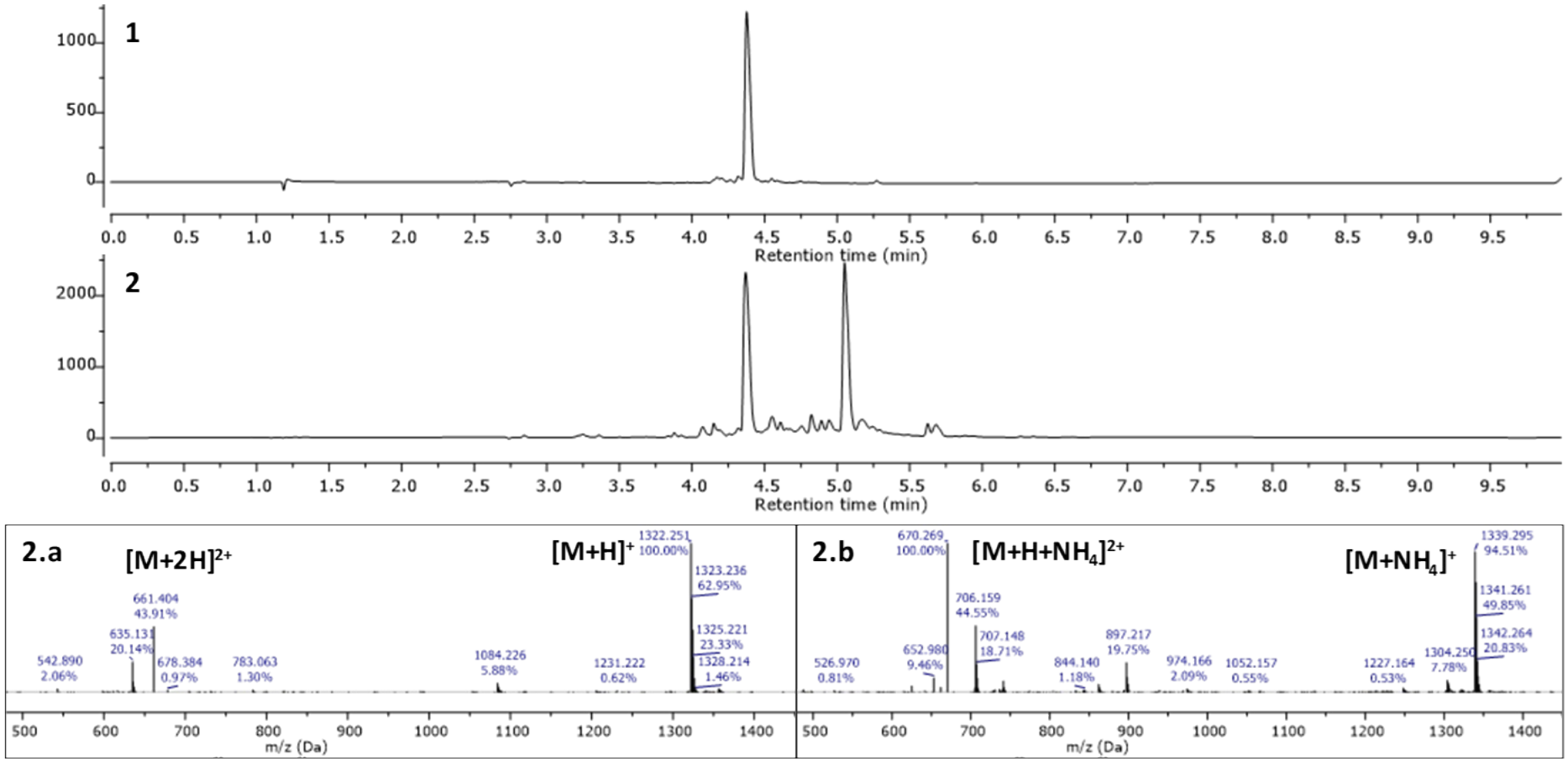

Figure S5. LC ESI-MS trace of the trimer (**1**) and its complexed form (**2**). **2.a** displays the ESI MS spectra of the LC peak at a retention time of 4.36 min. **2.b** shows the ESI MS spectra of the LC peak at a retention time of 5.06 min. The mass corresponds to the trimer without the nickel ion.

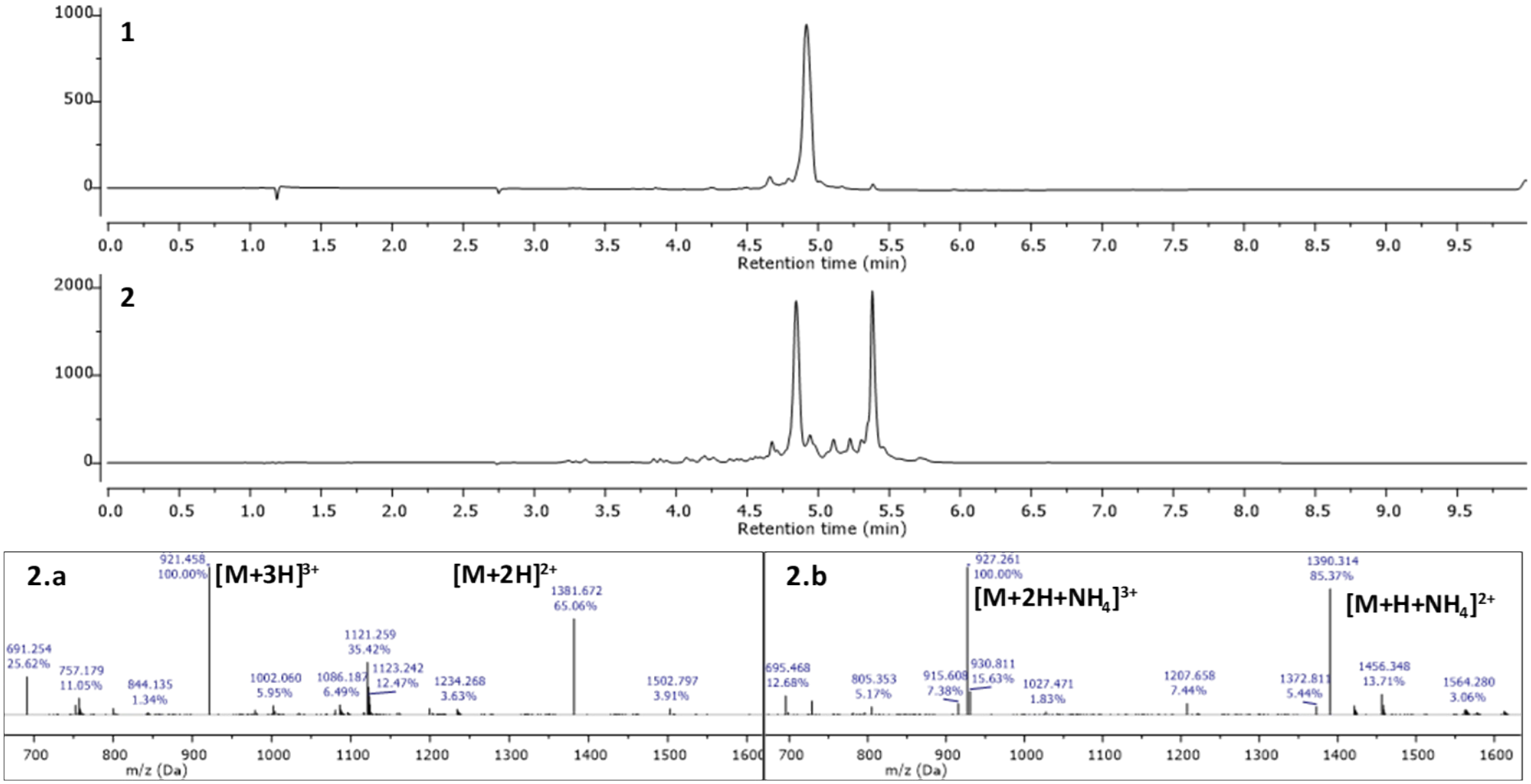

Figure S6. LC ESI-MS trace of the sequence S1,7 (**1**) and its compacted form (**2**). **2.a** shows the ESI MS spectra of the LC peak at a retention time of 4.36 min. **2.b** displays the ESI MS spectra of the LC peak at a retention time of 5.06 min. The mass corresponds to the trimer without the nickel ion.

NMR

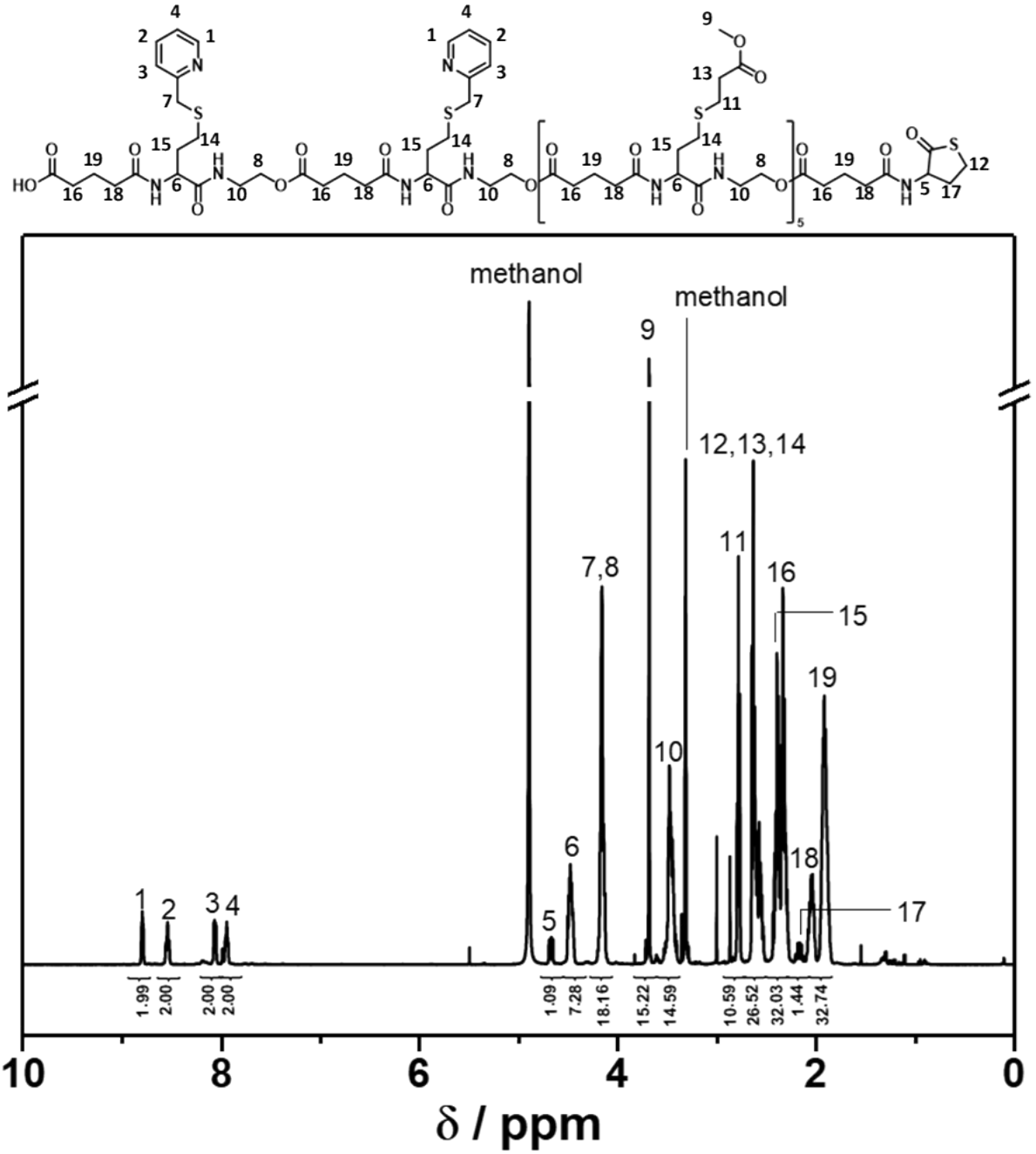

Figure S7. ^{1}H-NMR of the sequence S1,2 (500MHz, methanol-d_4).

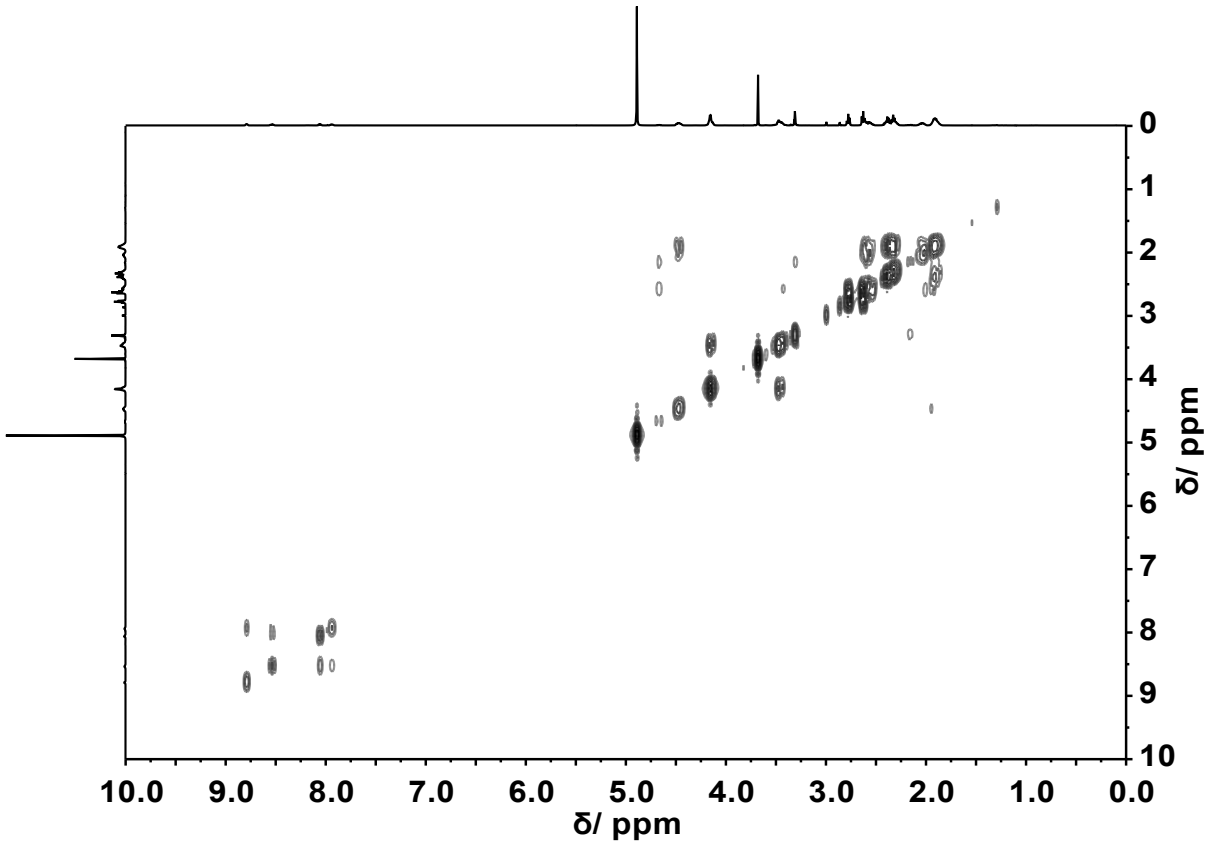

Figure S8. Correlation spectroscopy (COSY) spectra of S1,2 (500MHz, methanol-d_4).

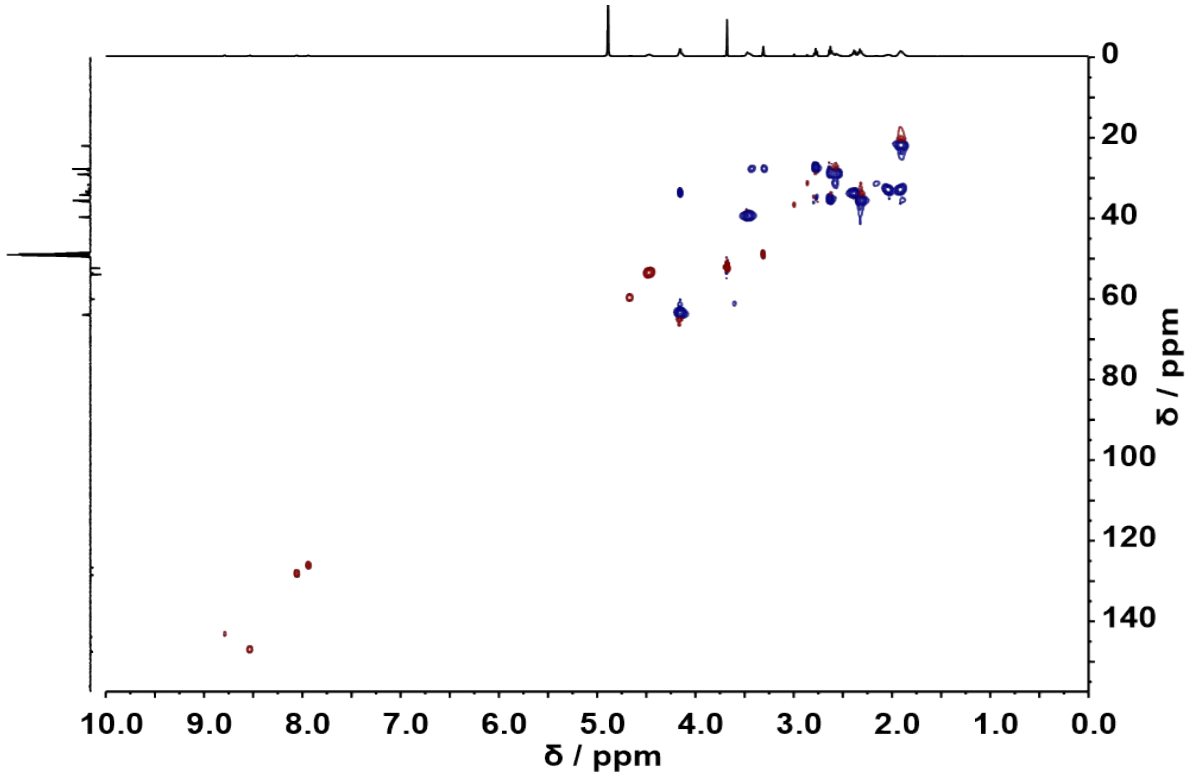

Figure S9. Heteronuclear single quantum coherence spectroscopy (HSQC) spectra of the sequence S1,2 (500MHz, methanol-d_4).

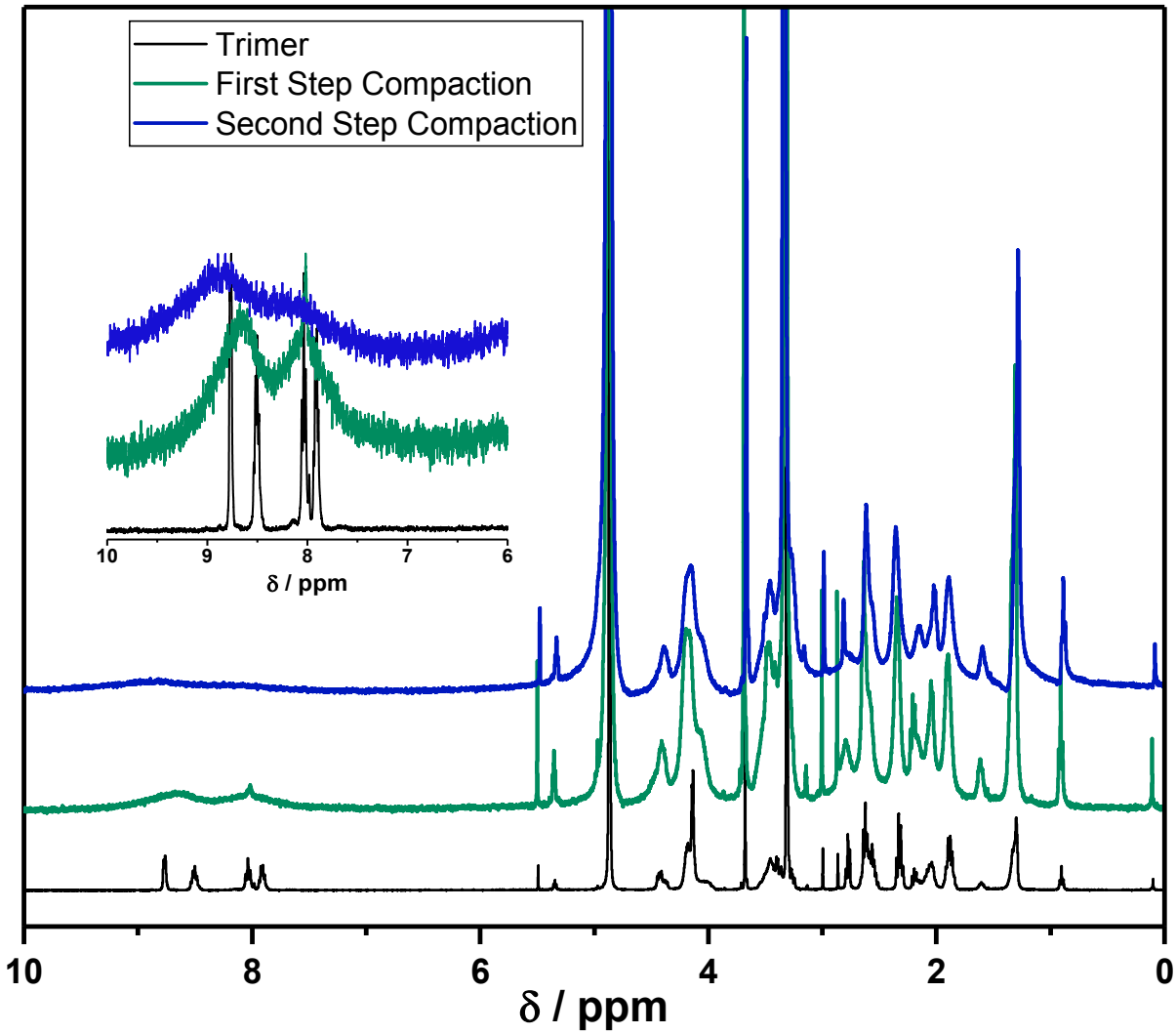

Figure S10. Full ^{1}H-NMR (400 MHz, methanol-d_4) spectra of the trimer (black), reacted with $Cu(ClO_4)_2$ (green) and after the addition of NaCl (blue).

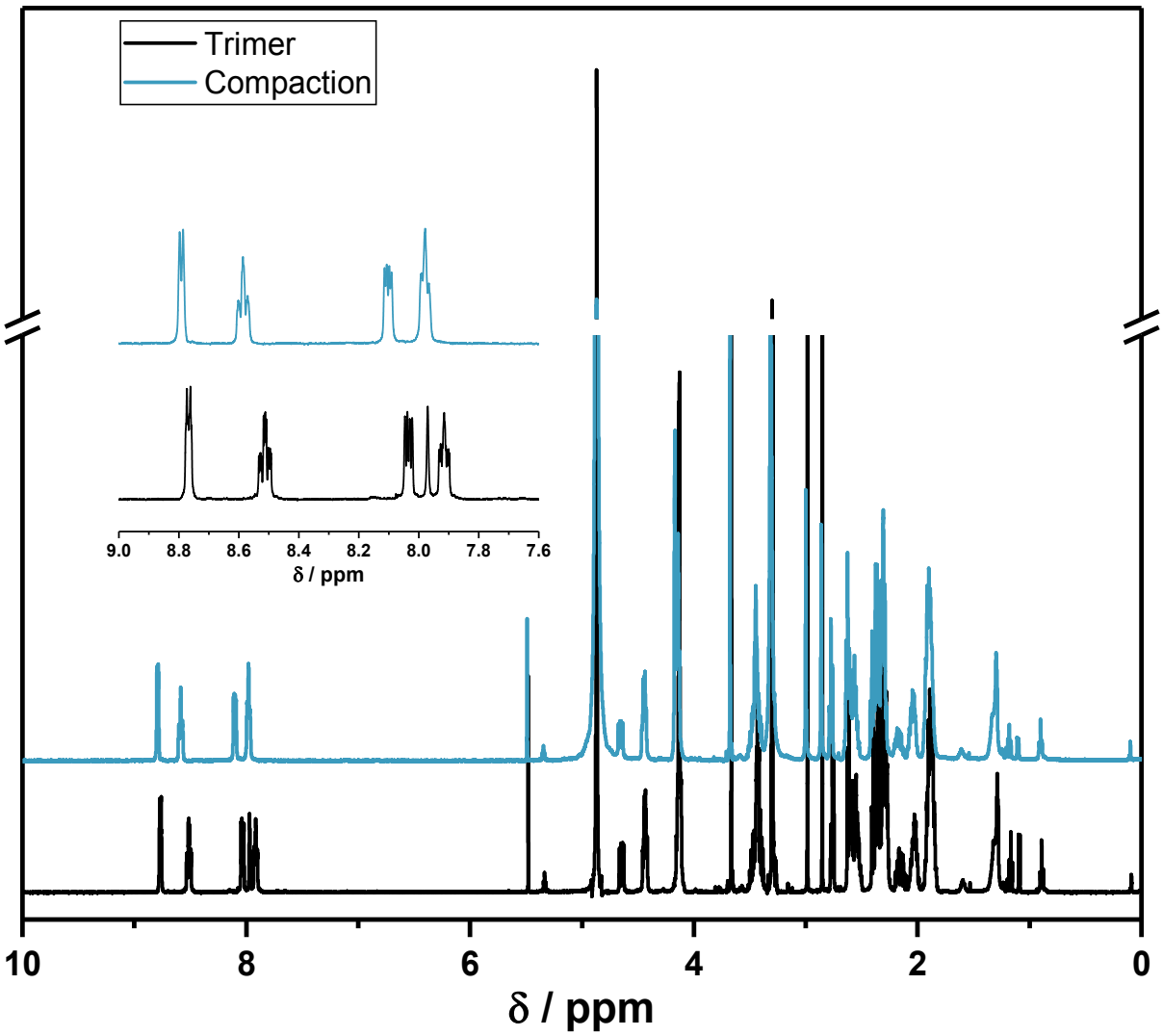

Figure S11. Full ^{1}H-NMR (500 MHz, methanol-d_4) spectra of the trimer (black) and its Ni(II)-SCNP (turquoise).

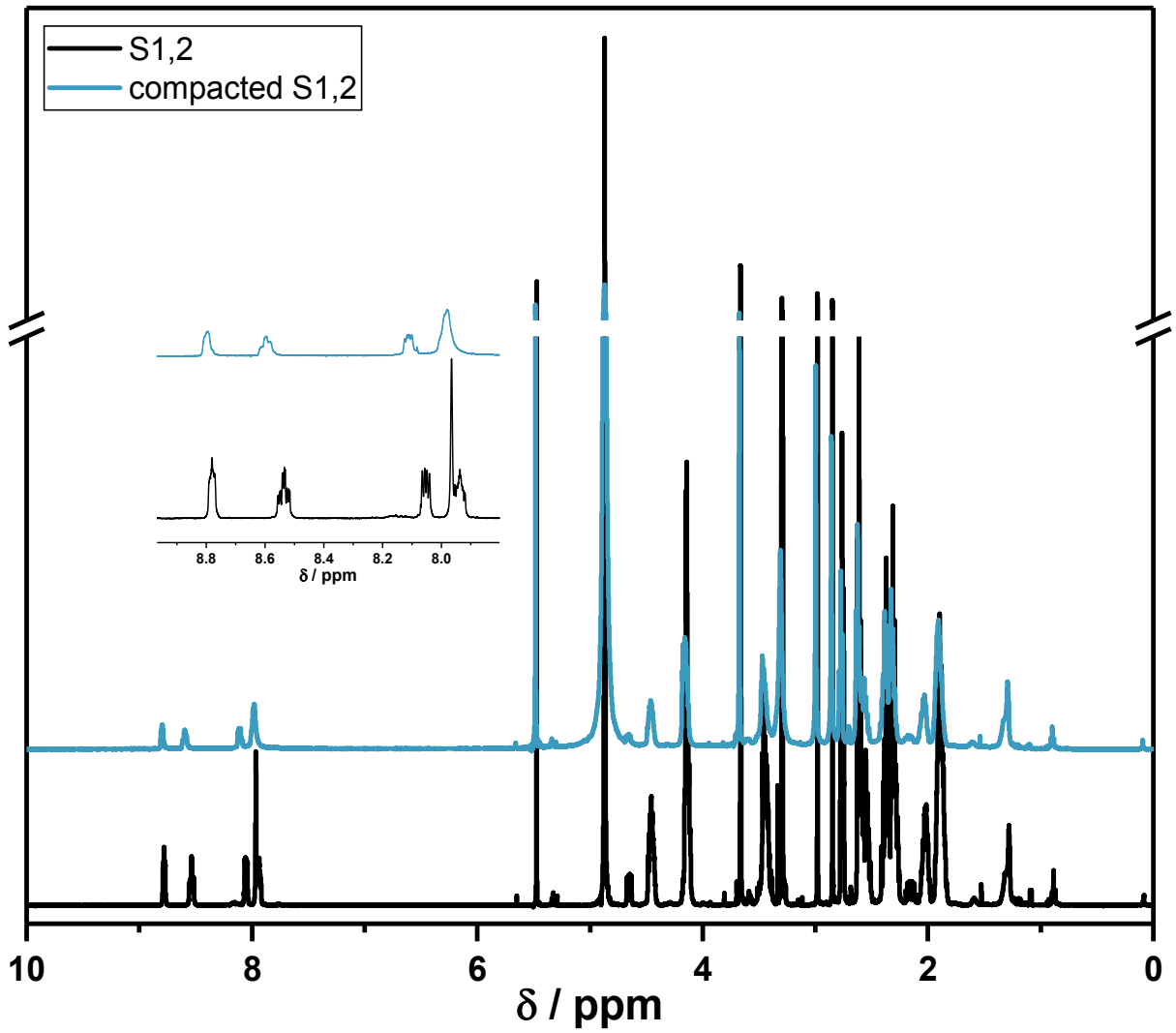

Figure S12. Full ^{1}H-NMR and zoom of aromatic region (500 MHz, methanol-d_4) of the heptamer S1,2 (black) and its complexed form (turquoise).

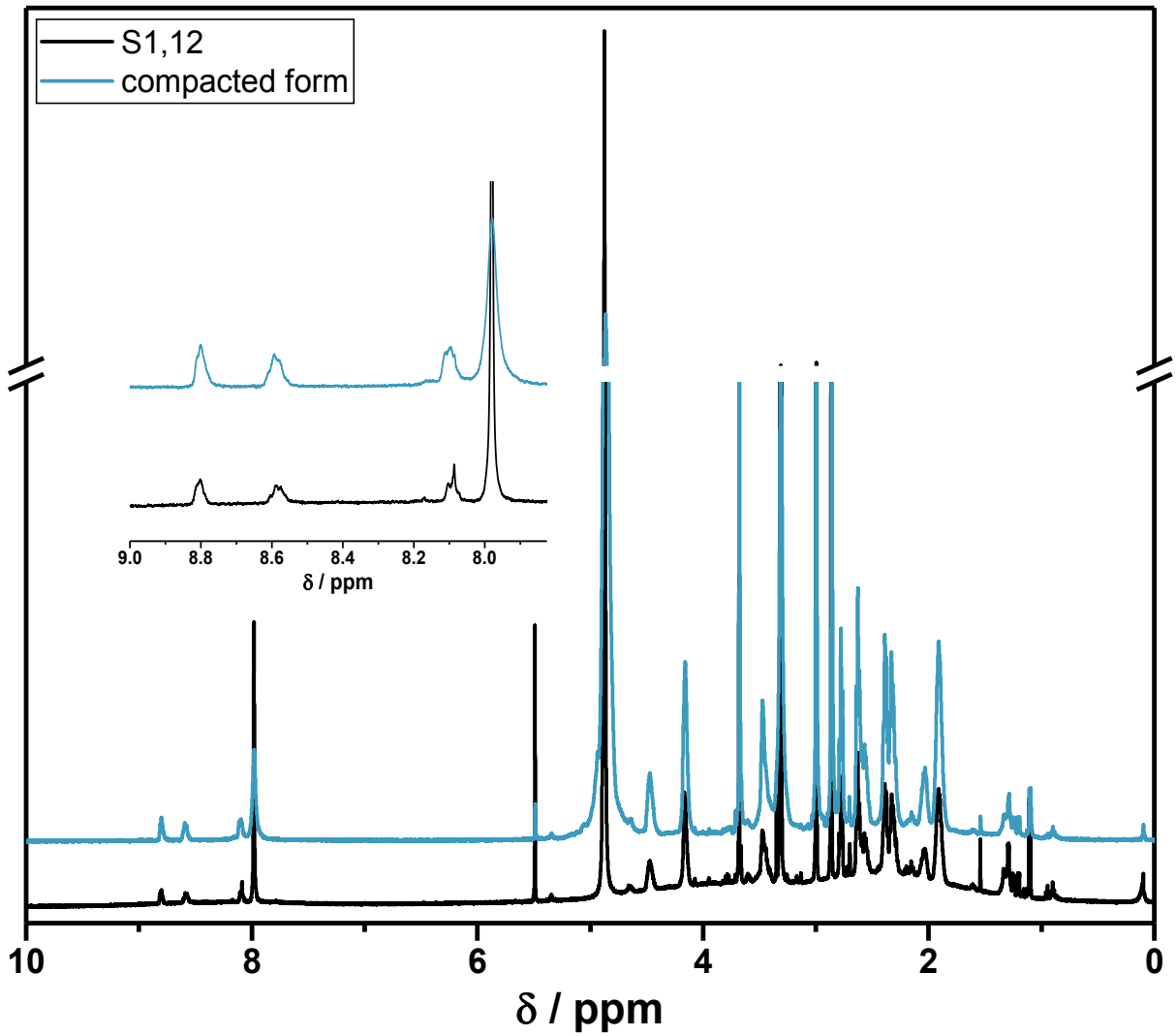

Figure S13. ^{1}H-NMR and zoom of aromatic region (500 MHz, methanol-d_4) of the sequence S1,12 (black) and its compacted form (turquoise).

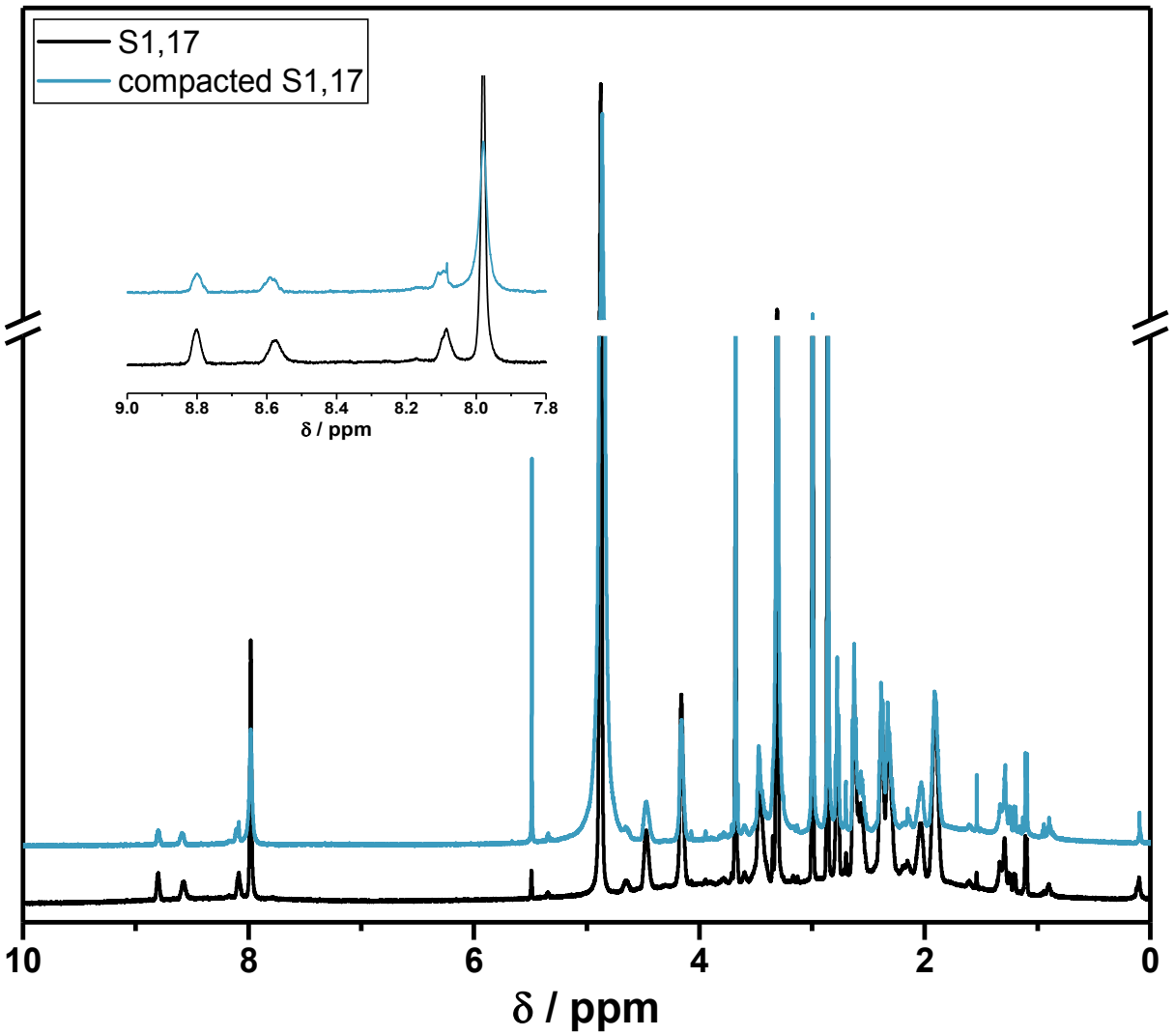

Figure S14. ^{1}H-NMR and zoom of aromatic region (500 MHz, methanol-d_4) of the sequence S1,17 (black) and its compacted form (turquoise).

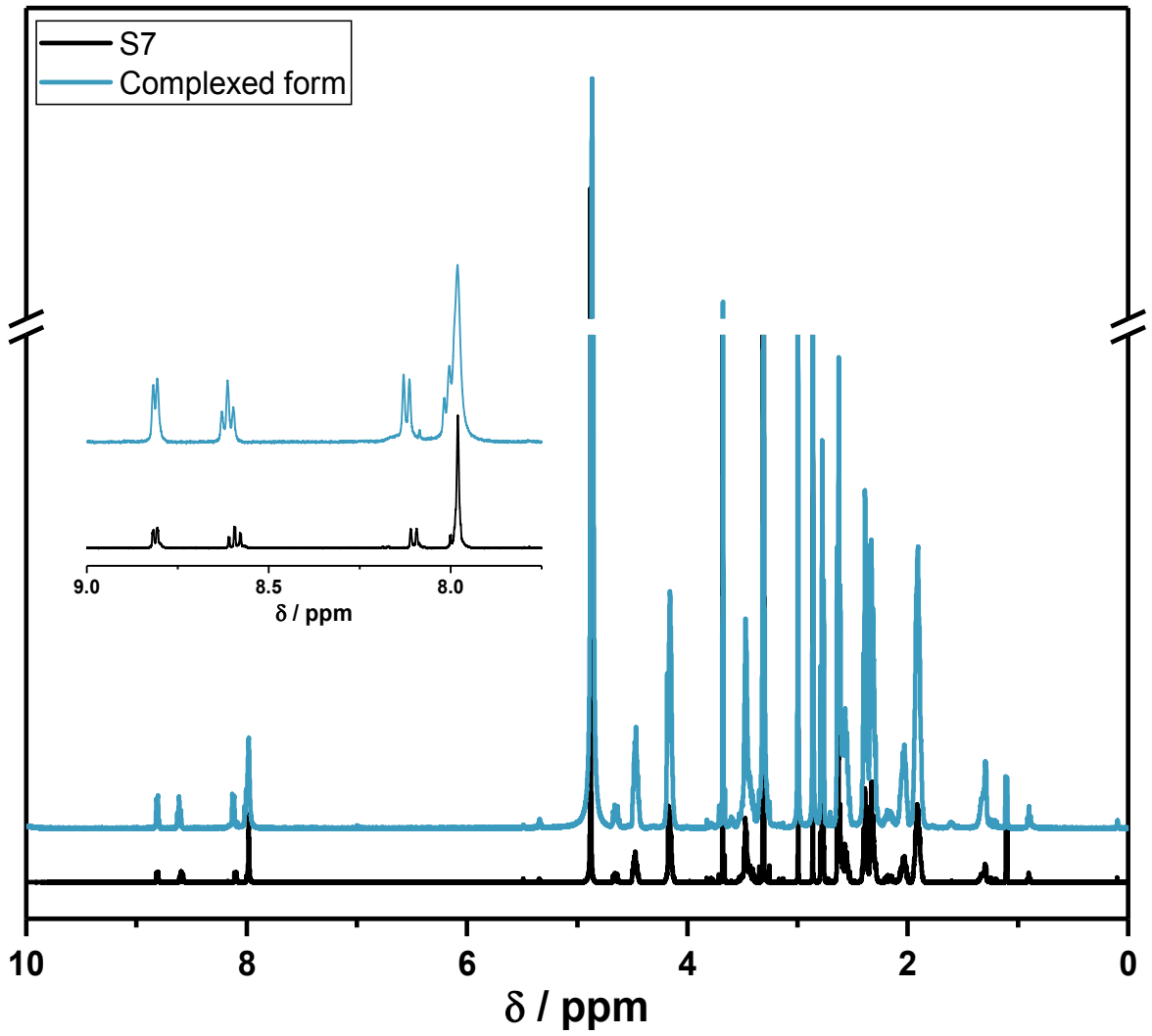

Figure S15. ^{1}H-NMR and zoom of aromatic region (500 MHz, methanol-d_4) of the reference sequence S7 (black) and its complexed form (turquoise).

DOSY

All DOSY measurements were performed using a Bruker Avance II 500 at 500 MHz in methanol-d_4

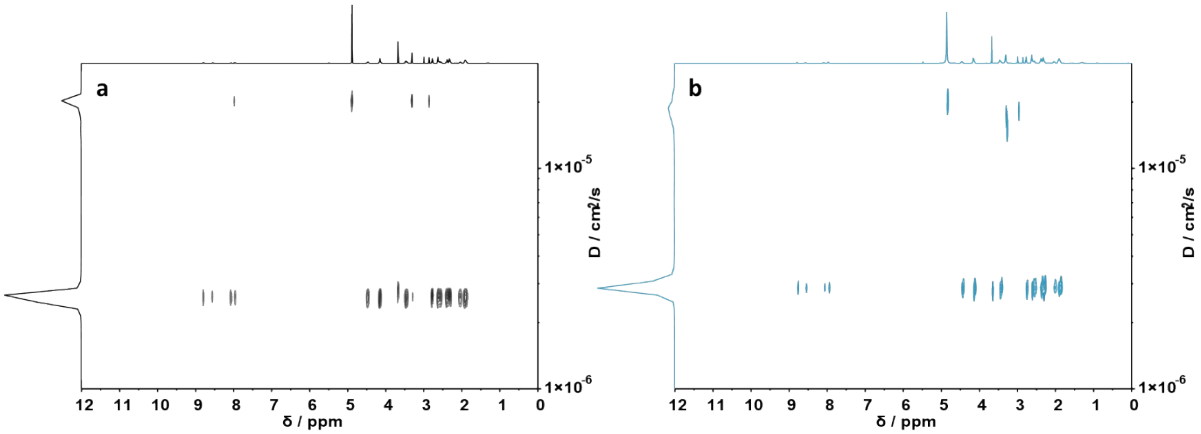

Figure S16. (a) DOSY spectra of S1,2 and (b) of its compacted form.

(unless otherwise stated).

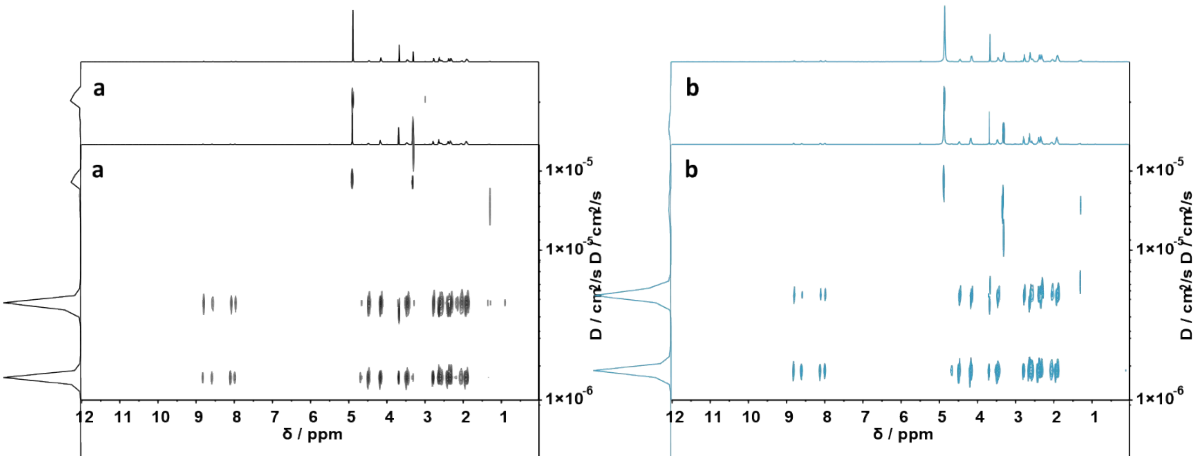

Figure S17. (a) DOSY spectra of S1,3 and (b) of its compacted form.

Figure S18. DOSY spectra of (a) S1,4 and (b) its complexed structure.

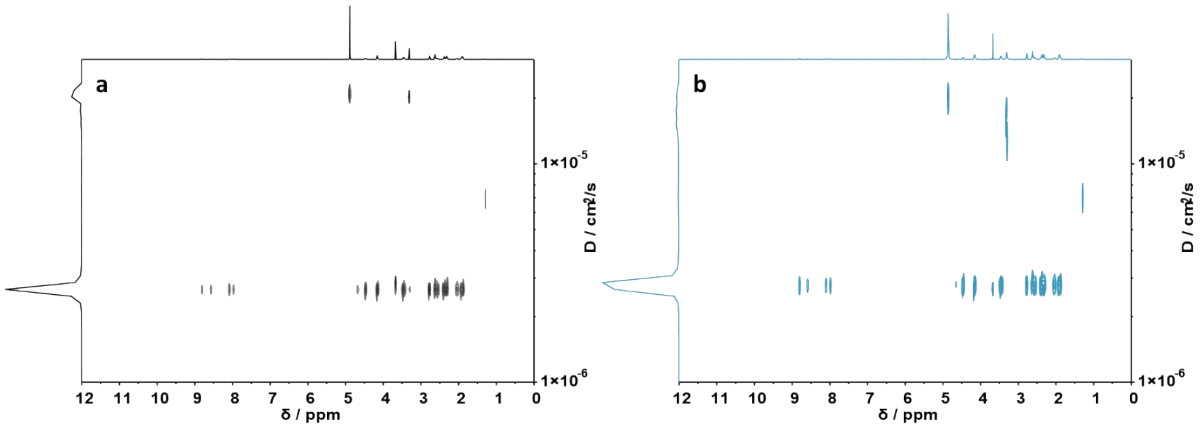

Figure S19. DOSY spectra of (a) S1,5 and (b) its Ni(II)-SCNP.

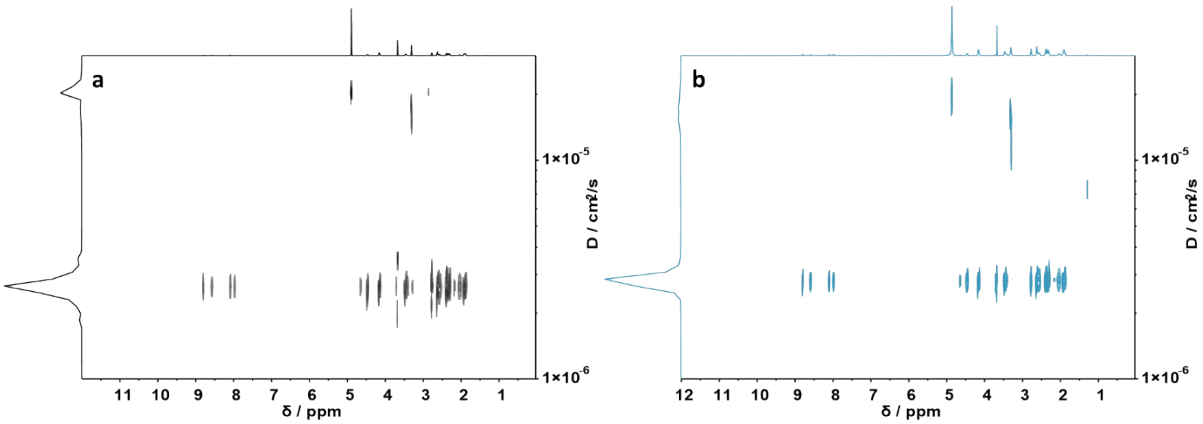

Figure S21. DOSY spectra of (a) S1,7 and (b) its complexed form.

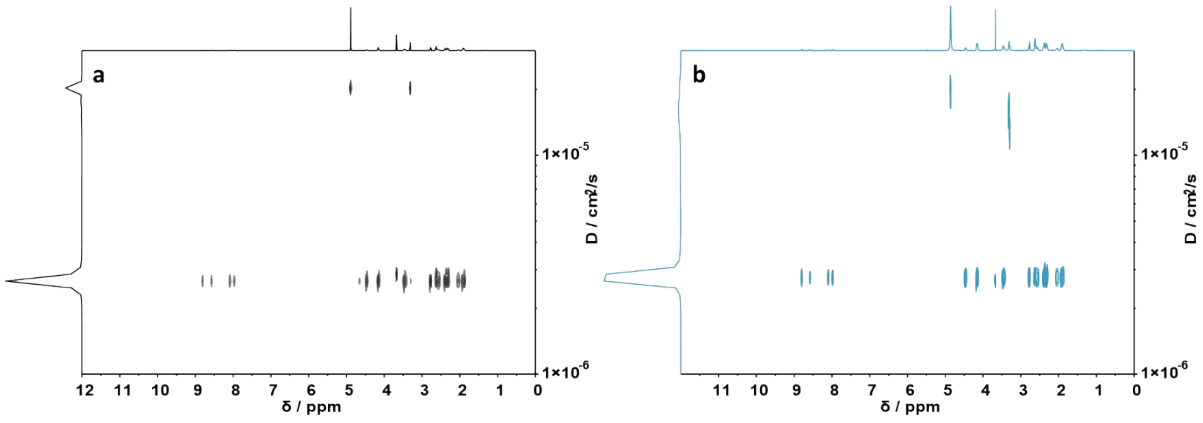

Figure S20. DOSY spectra of (a) S1,6 and (b) its compacted structure.

In the following figures (Figure S17 to Figure S28), the intensity ***I*** of the observed signals in the DOSY measurements is plotted logarithmically against the gyromagnetic ratio ***γ*** of the observed nucleus,

the gradient strength ***G***, the length of the gradient ***δ*** and the diffusion time ***Δ*** to obtain the diffusion coefficient ***D*** through the slope of the curve.

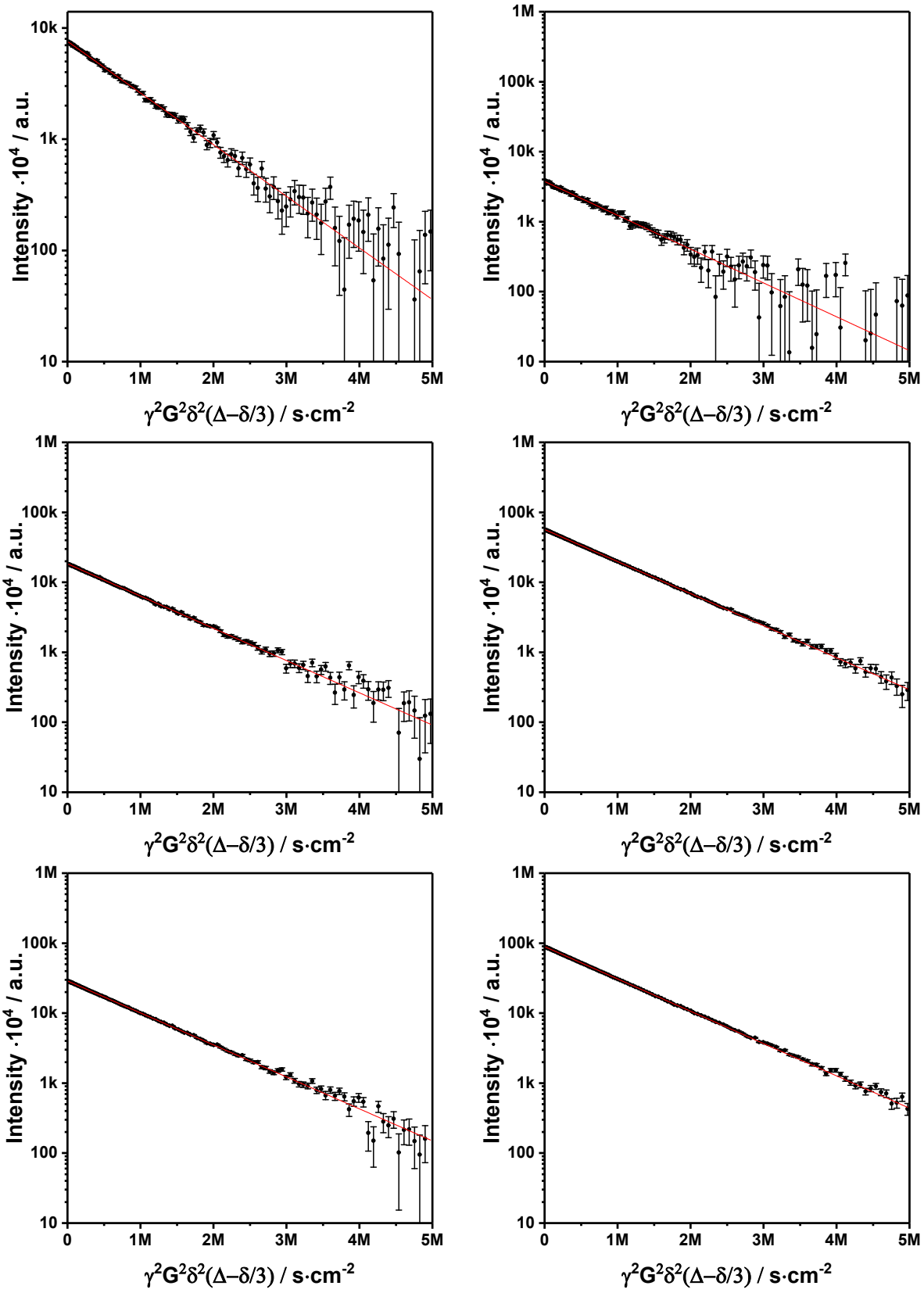

Figure S22. Sequence S1,2.

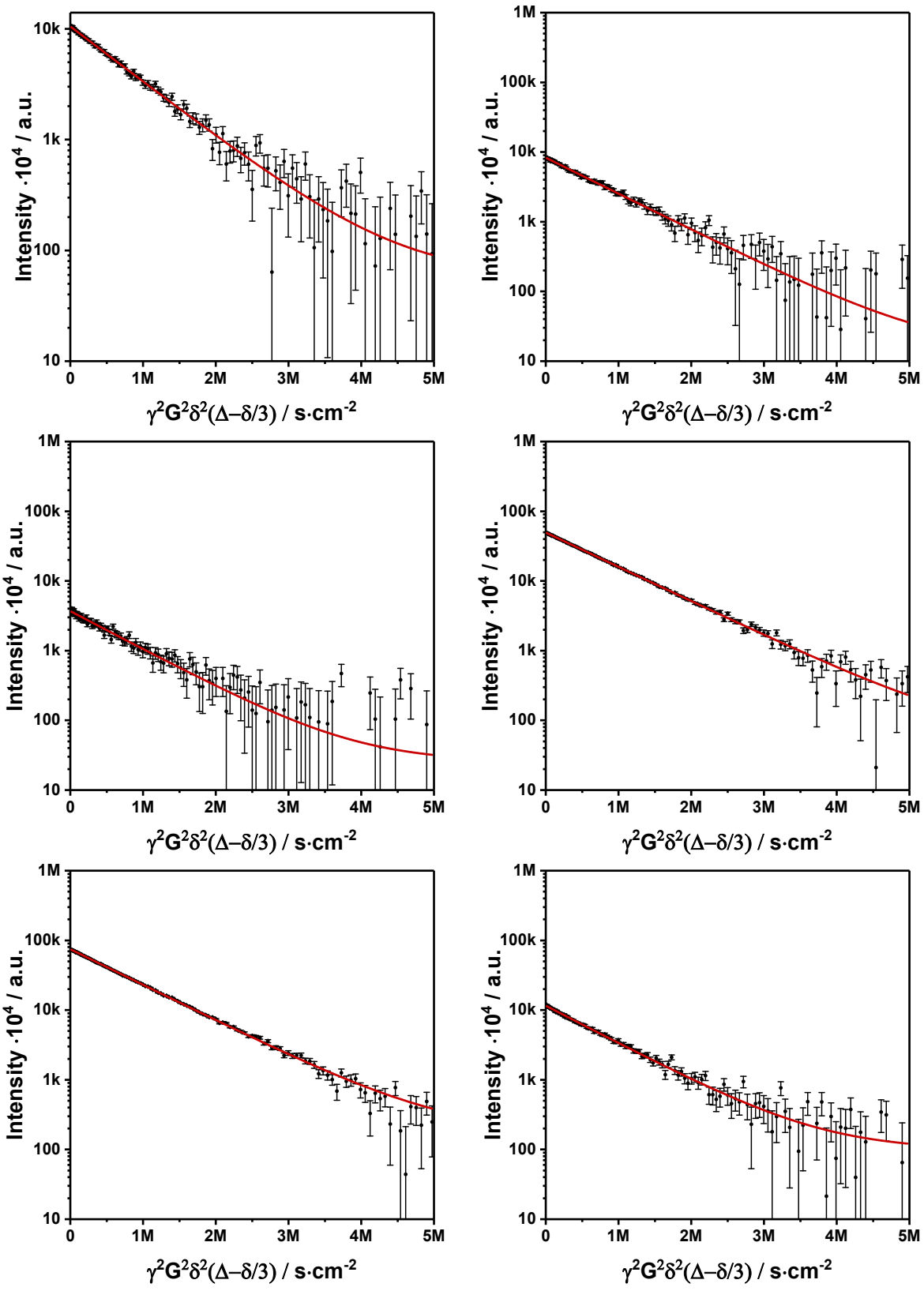

Figure S23. Complexed sequence S1,2.

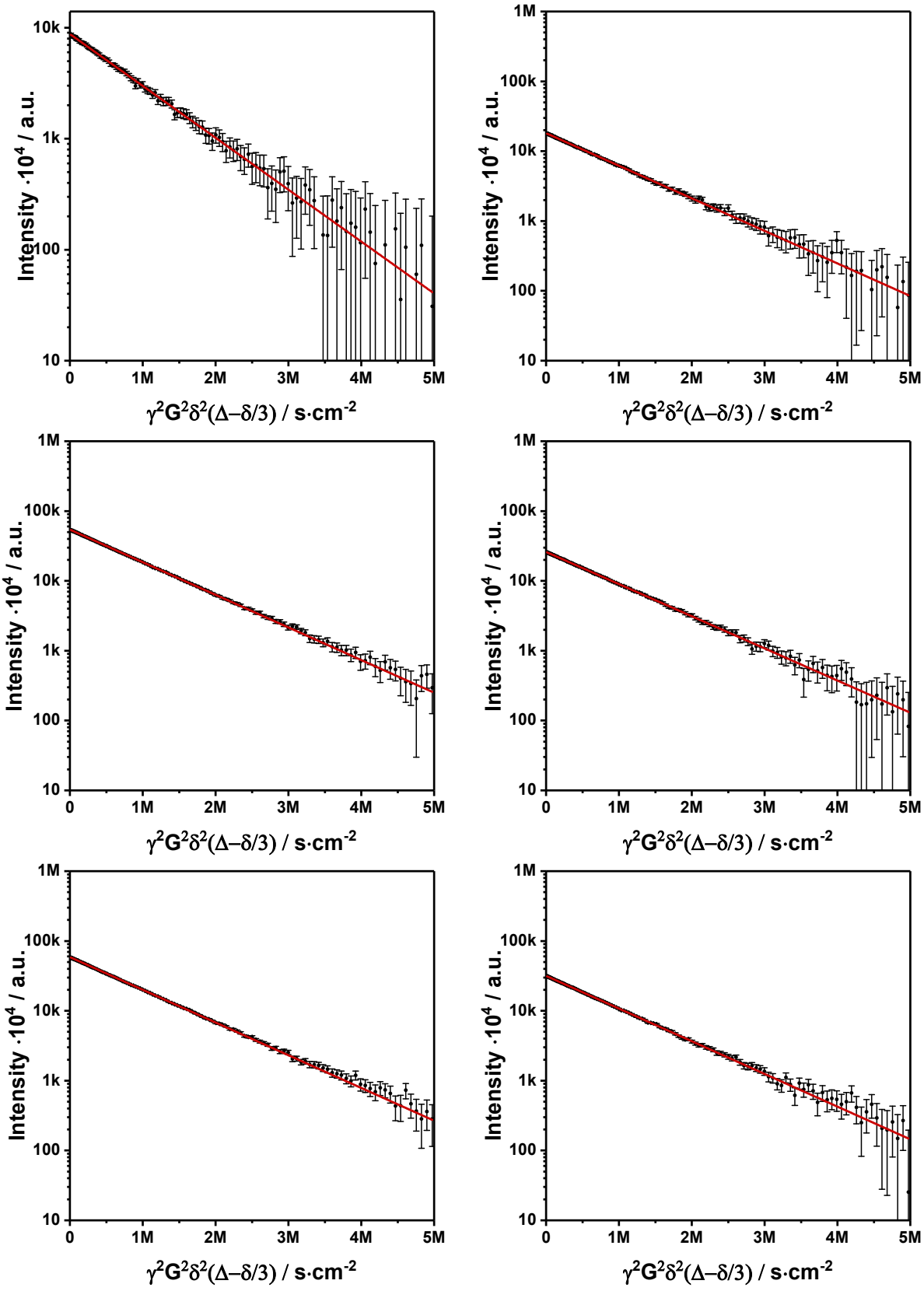

Figure S24. Sequence S1,3.

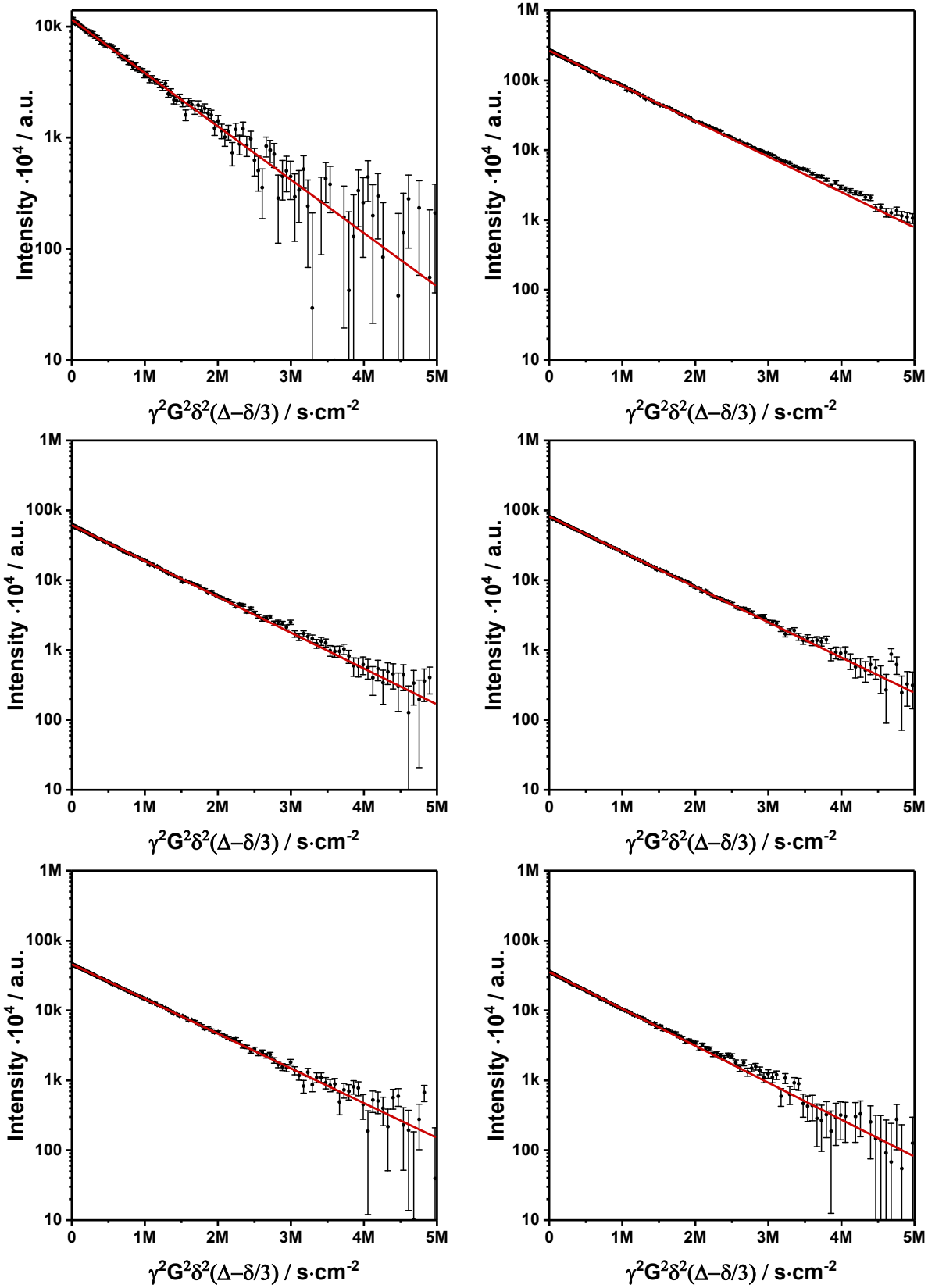

Figure S25. Complexed sequence S1,3.

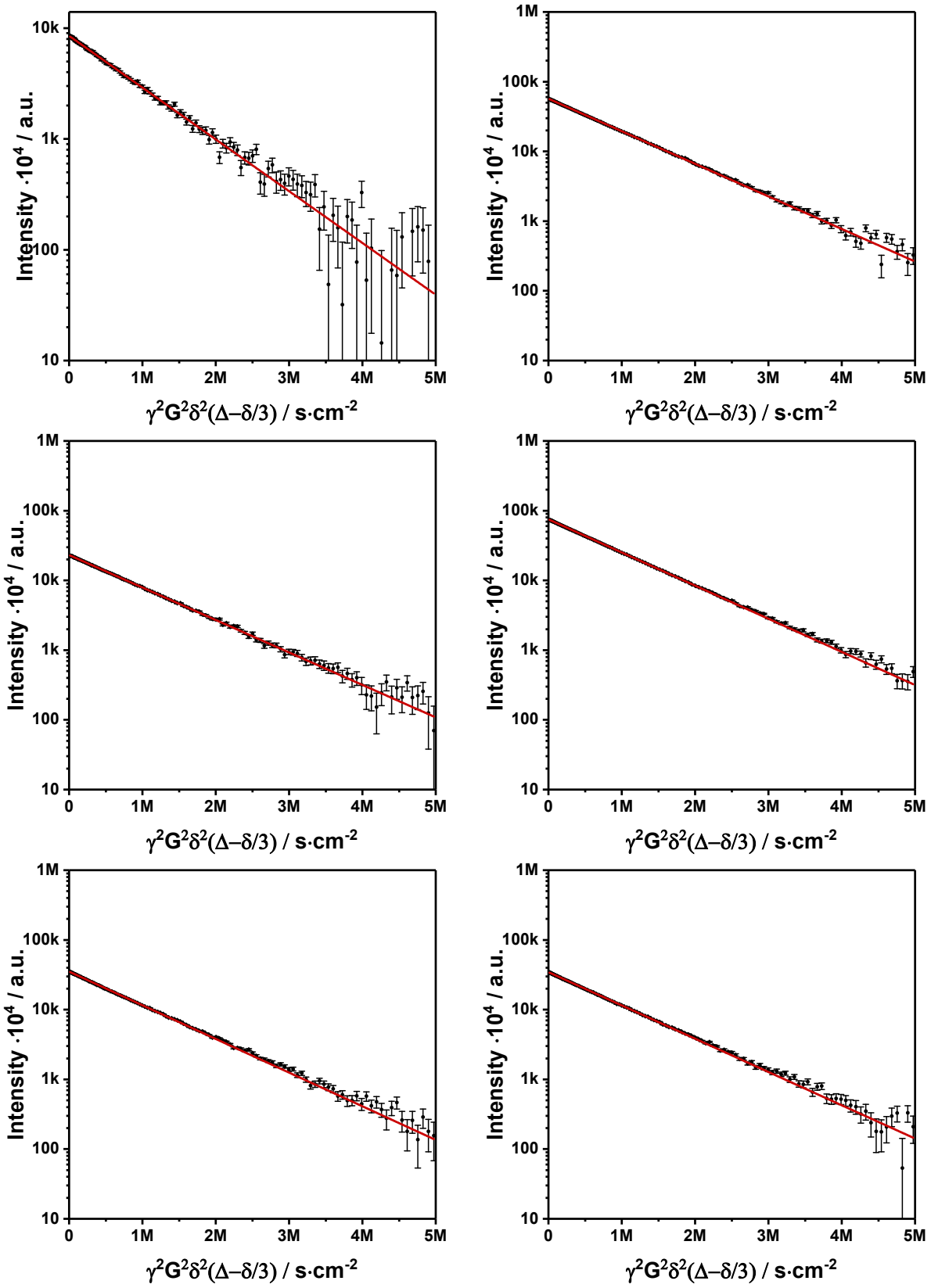

Figure S26. Sequence S1,4.

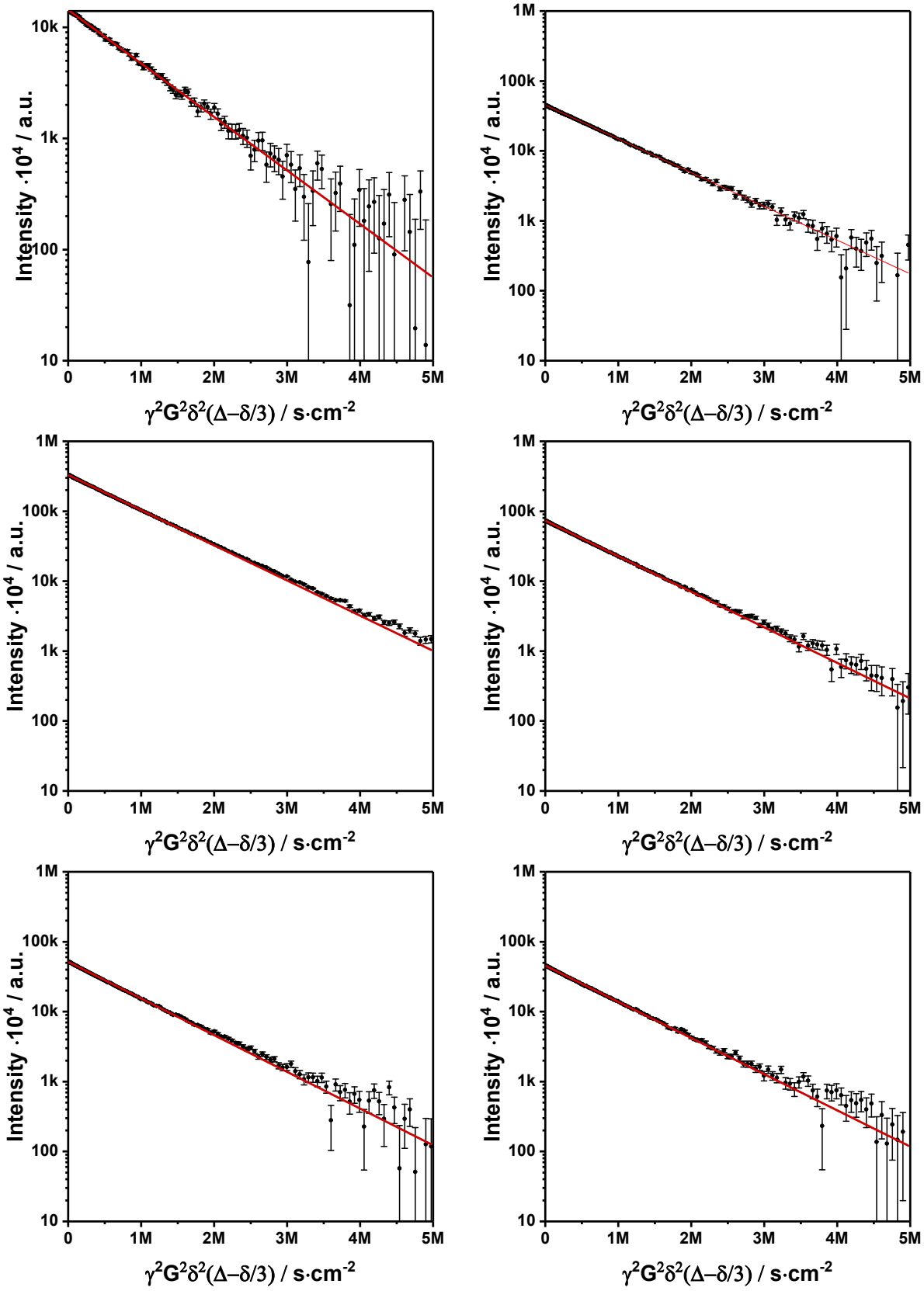

Figure S27. Complexed sequence S1,4.

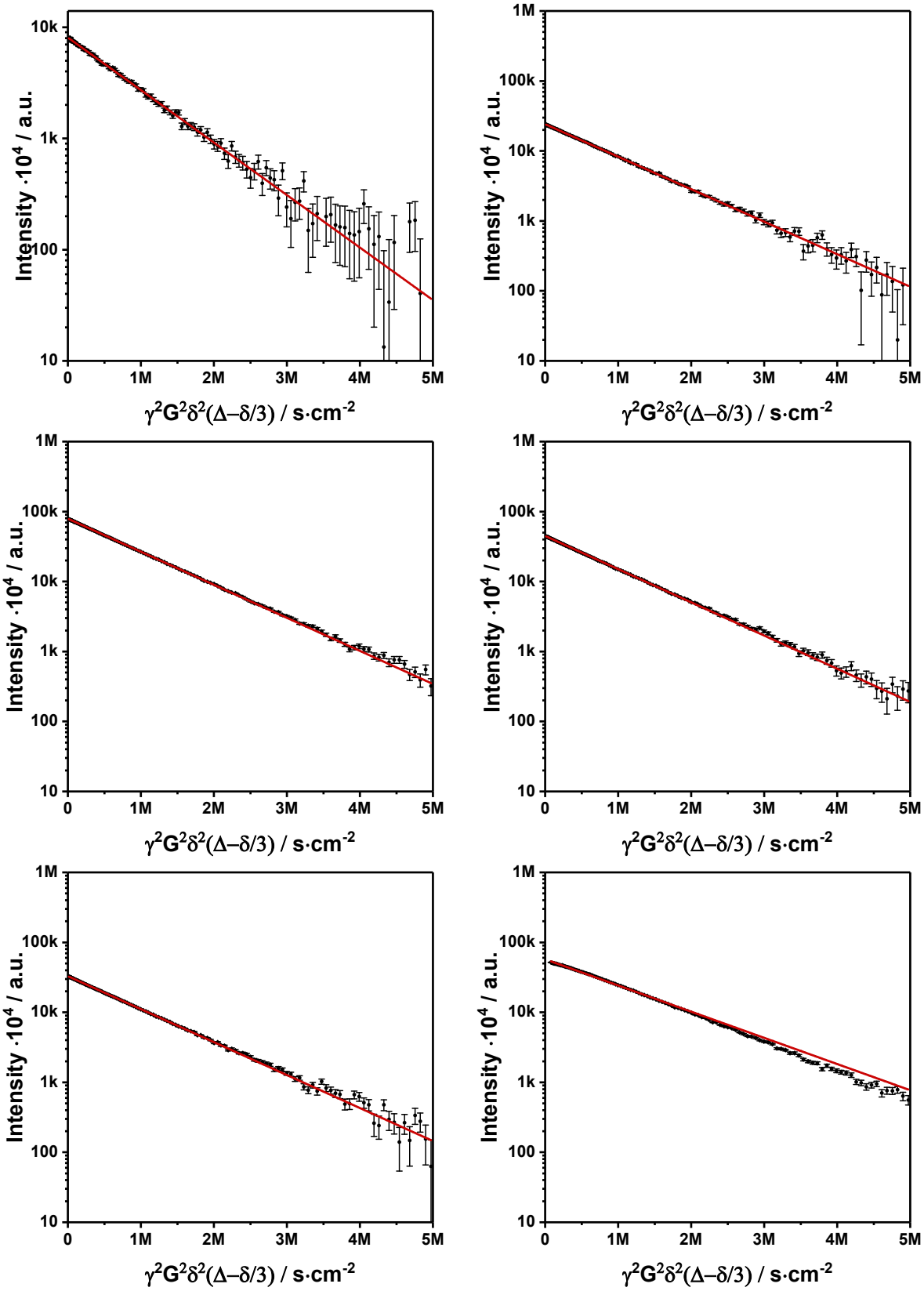

Figure S28. Sequence S1,5.

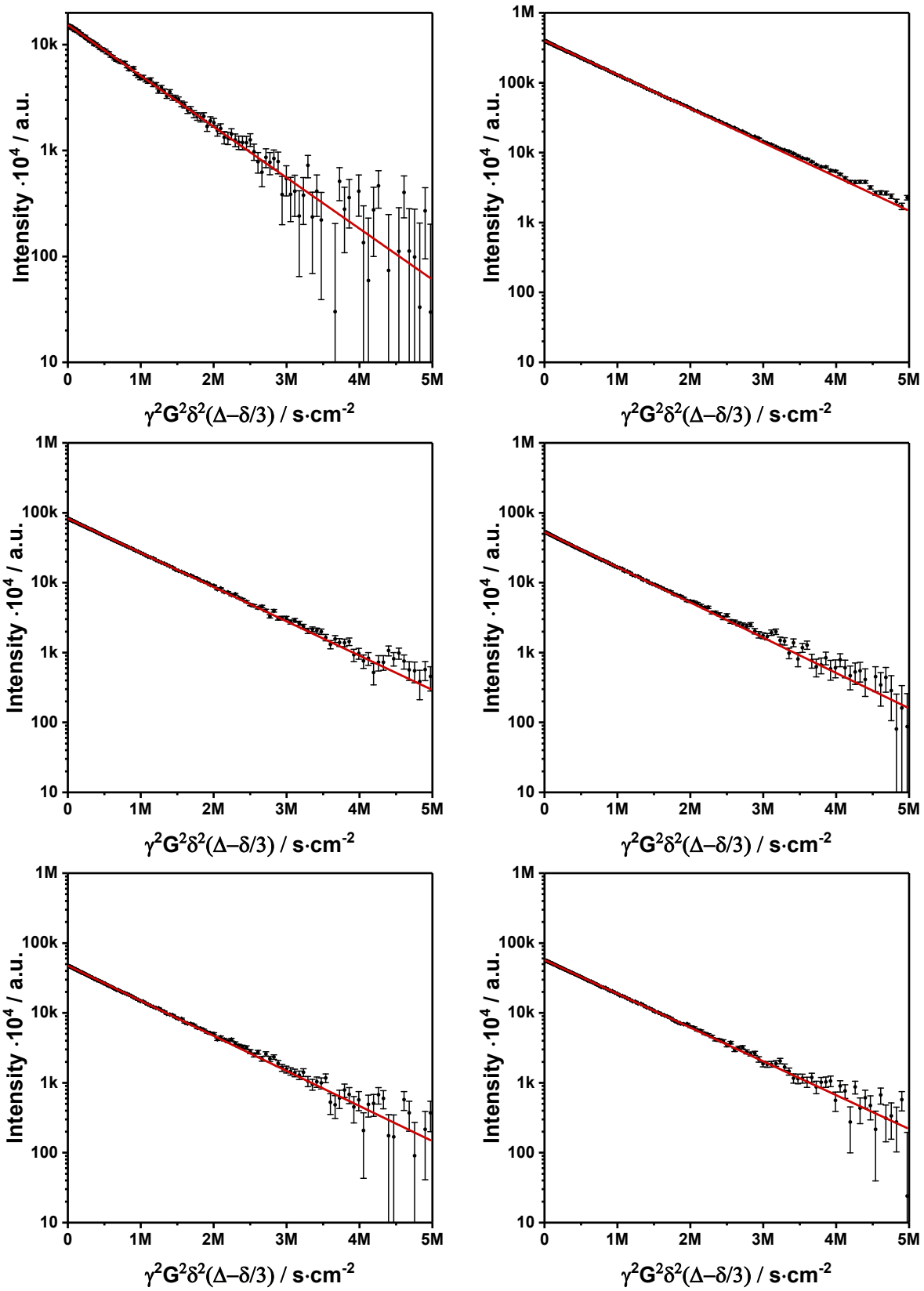

Figure S29. Complexed sequence S1,5.

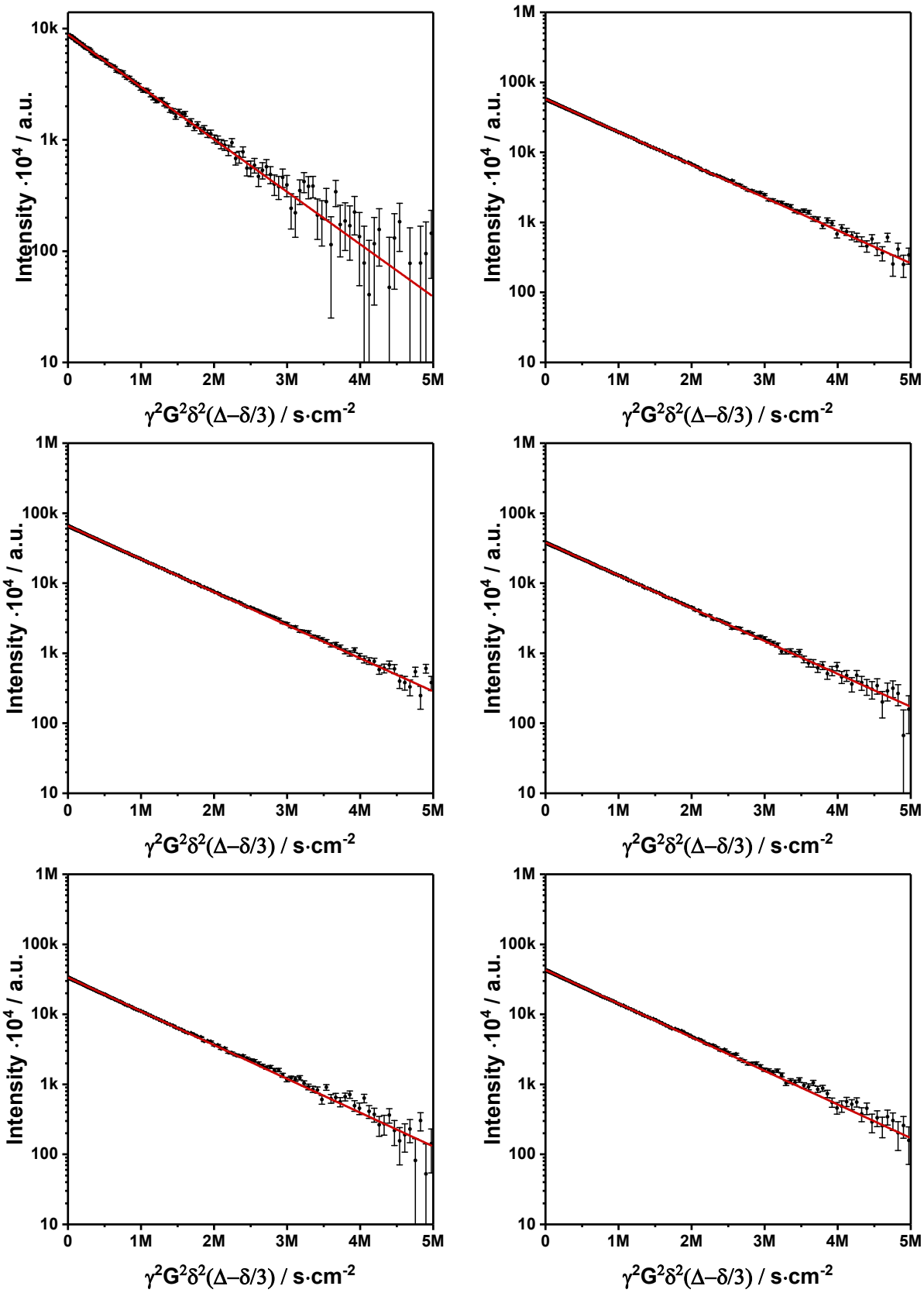

Figure S30. Sequence S1,6.

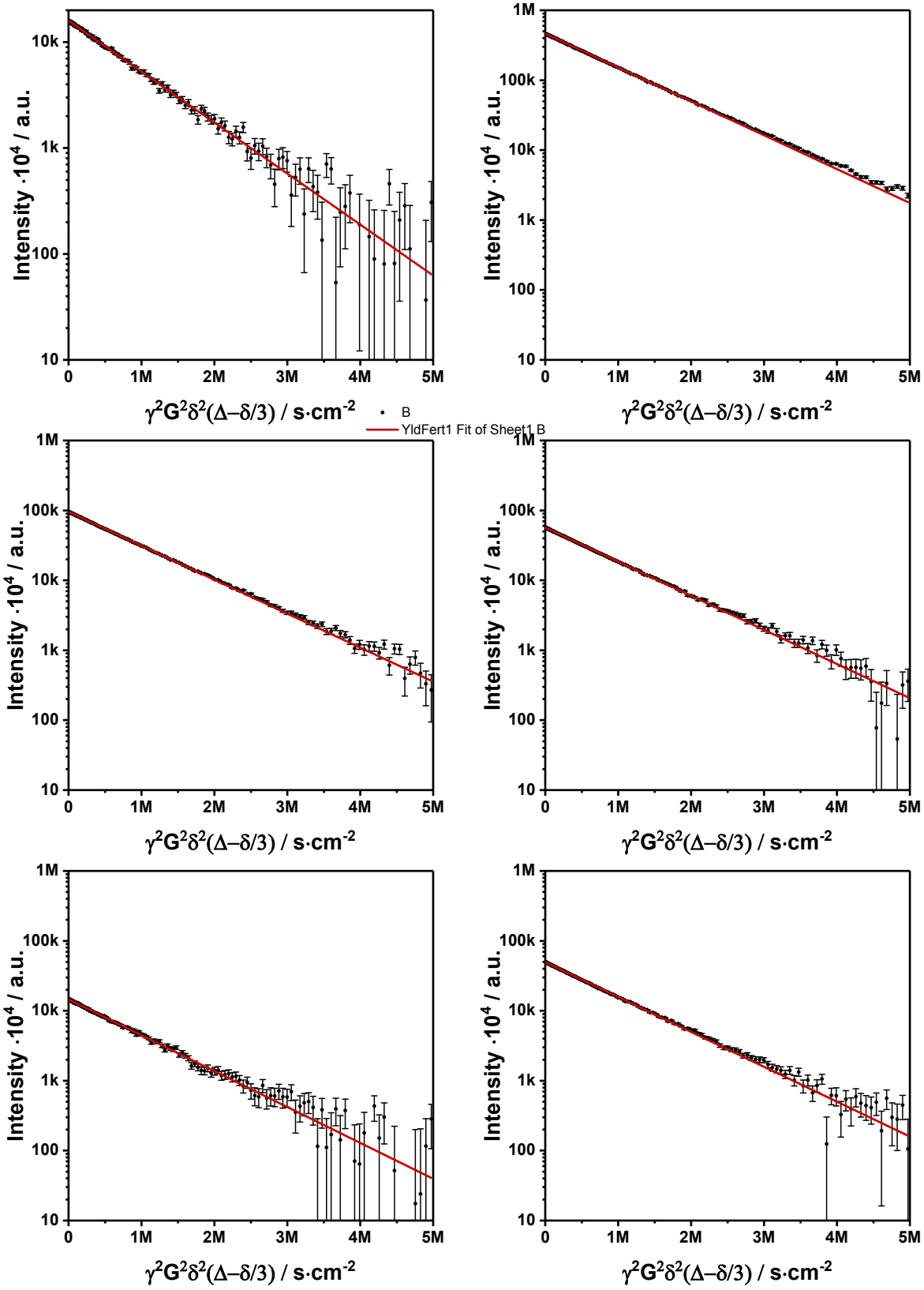

Figure S31. Complexed sequence S1,6.

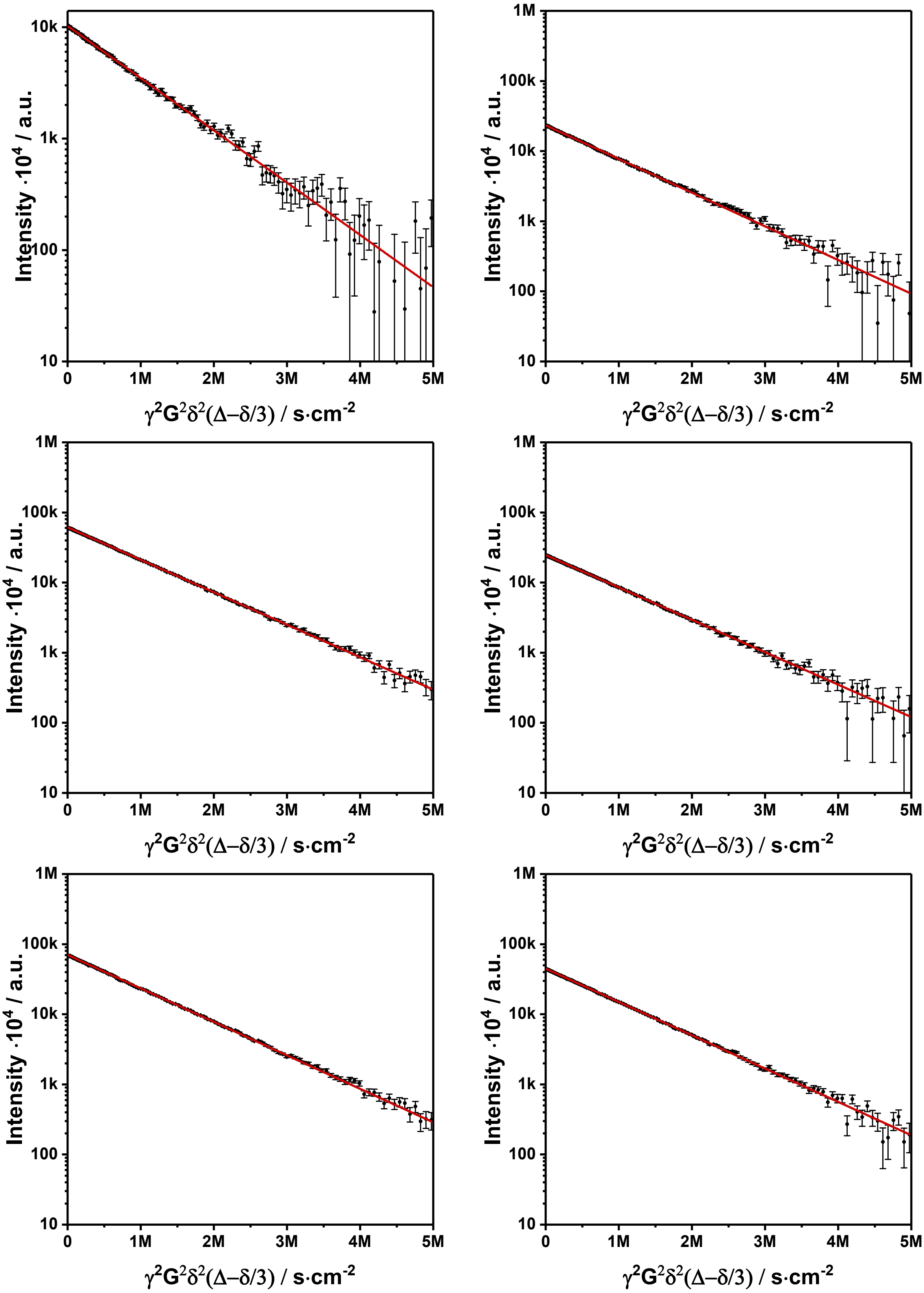

Figure S32. Sequence S1,7.

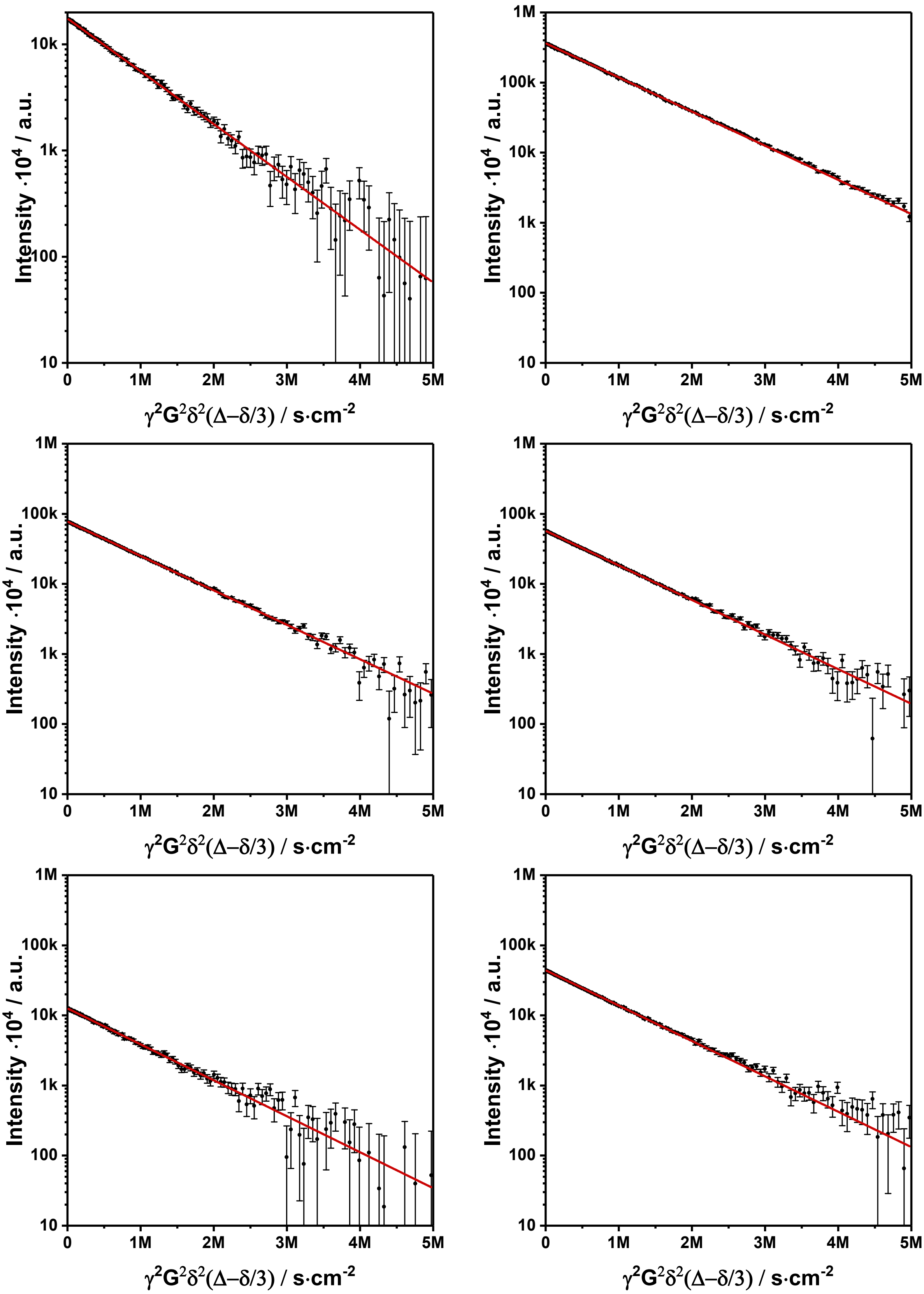

Figure S33. Complexed sequence S1,7.

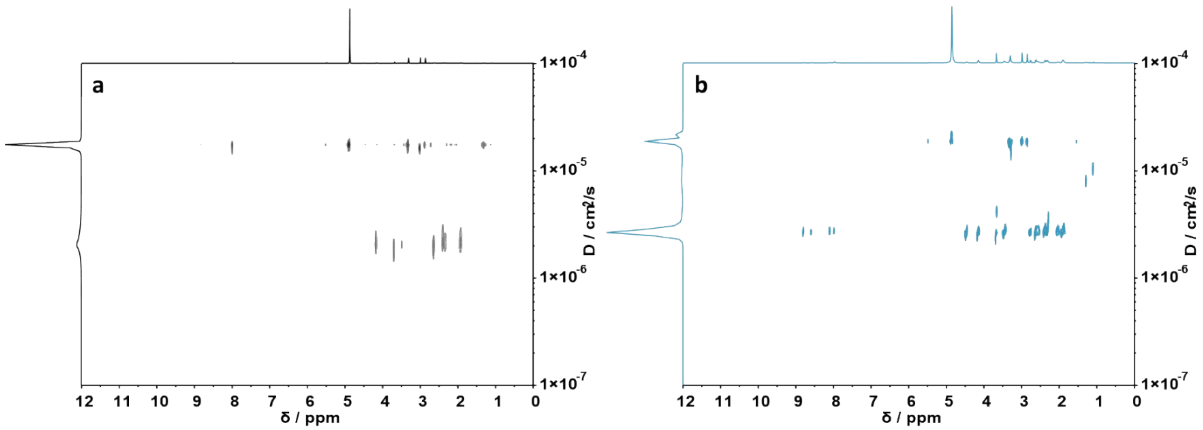

Figure S34. DOSY spectra of (a) S1,12 and(b) its compacted structure.

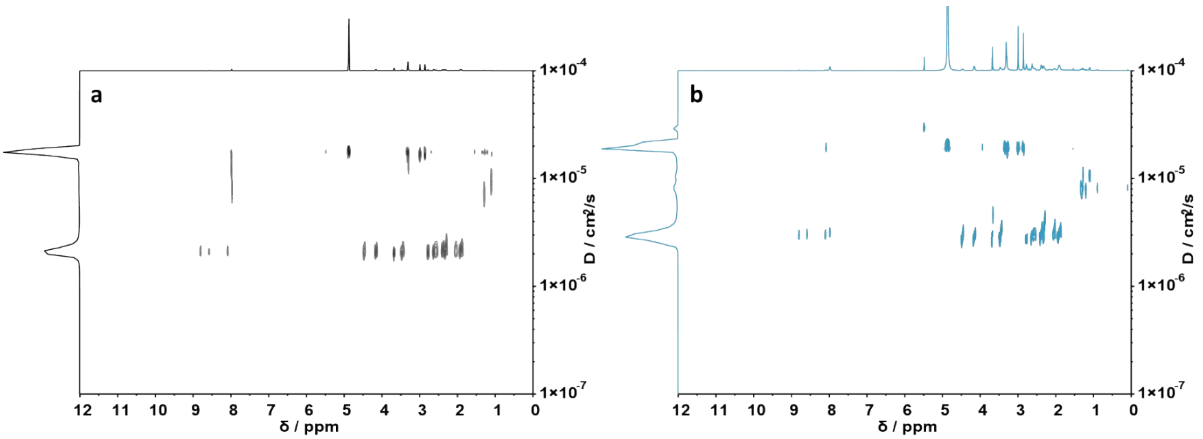

Figure S35. DOSY spectra of (a) S1,17 and (b) its compacted structure.

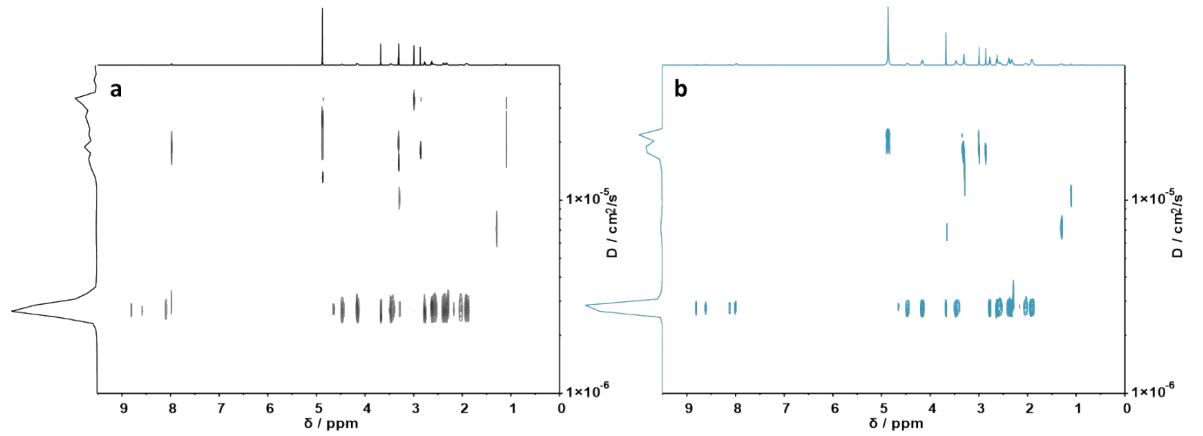

Figure S36. DOSY spectra of (a) S7 and (b) its complexed structure.

Table S11. Hydrodynamic radii for the sequences and their compacted structures obtained through the Stokes Einstein equation from the diffusion coefficient from the DOSY measurements. For S1,2 to S1,7 two measurements per sequence were conducted.

Sequence	R_h(oligomer) / nm	R_h(compacted) / nm	Compaction ratio / %
S1,2	1.39	1.27	8.3
	1.39	1.28	8.3
S1,3	1.36	1.27	6.7
	1.39	1.31	6.0
S1,4	1.36	1.30	4.2
	1.38	1.32	4.4
S1,5	1.35	1.30	3.1
	1.39	1.35	2.5
S1,6	1.35	1.31	2.7
	1.39	1.35	3.2
S1,7	1.37	1.30	5.0
	1.37	1.32	4.2
S1,12	1.72	1.39	18.8
S1,17	1.70	1.28	24.8
S7	1.28	1.32	

Temperature dependent DOSY

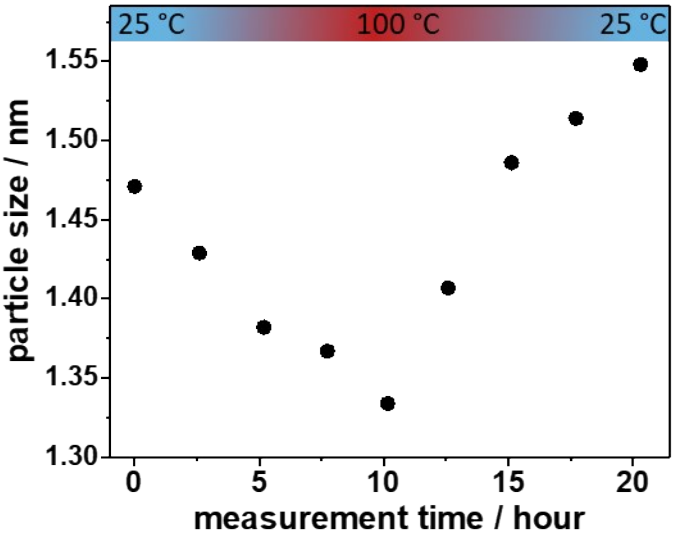

Figure S37. SCNP size depending on temperature. The compacted oligomer S1,7 was dissolved in *N,N*-dimethylformamide-d_7 and was measured at different temperature of 20 °C increments from 25 °C to 100 °C.

UV-Vis

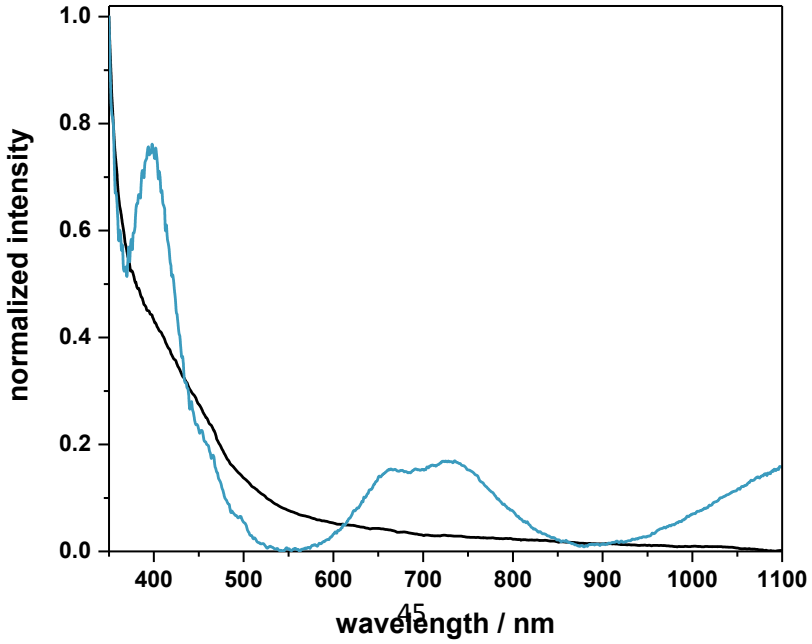

Figure S38. UV-Vis spectra from 350 to 1100 nm of sequence S1,2 (black) and its compacted form (turquoise) in methanol.

ESI-MS

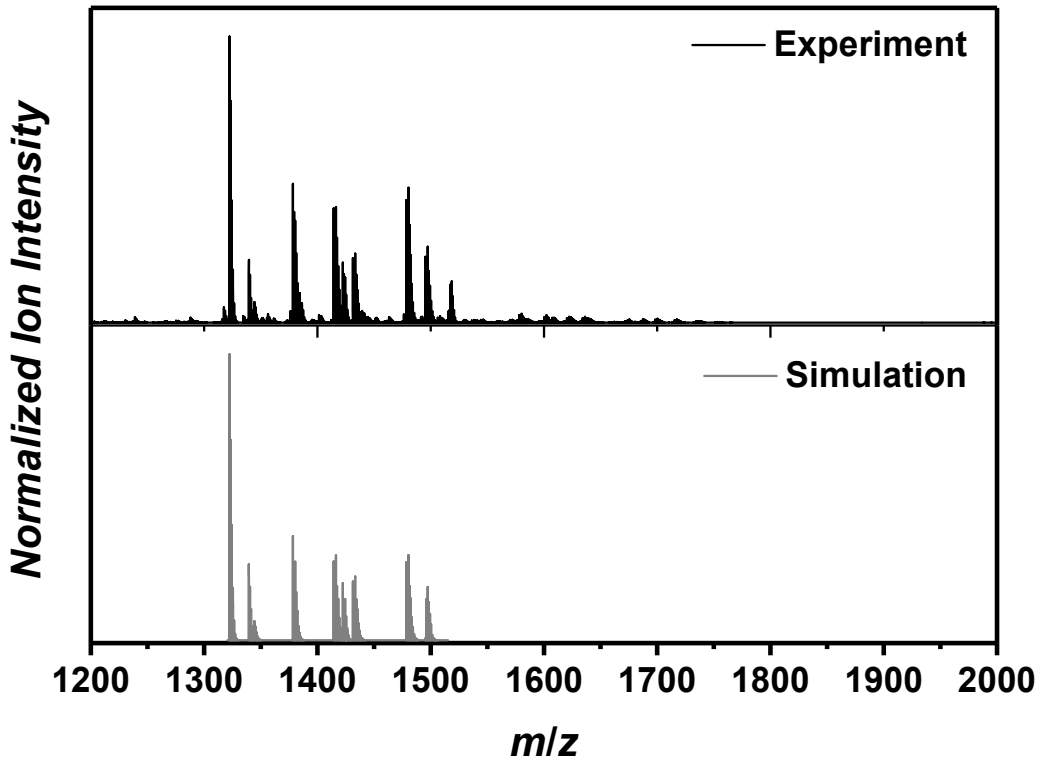

Figure S39. High resolution ESI Orbitrap mass spectrum of the trimer after the complexation with Ni(II) ions. On the top the experimental results were displayed and on the bottom the results of the simulations. Table S12 displays the assignment of the peaks.

Table S12. Assignment of the peaks of the trimer (Figure S39).

Structure	Sum Formula	m/z (exp)	m/z (theo)	Δm/z	Resolution
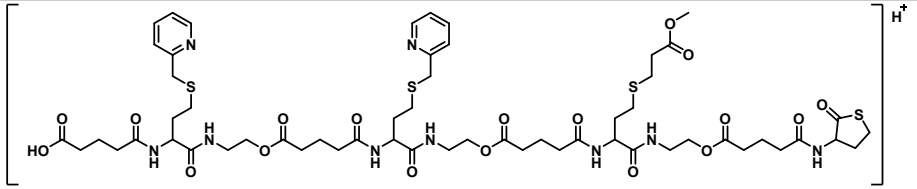	$C_{58}H_{84}N_9O_{18}S_4$	1322.4812	1322.4812	0.0000	61000
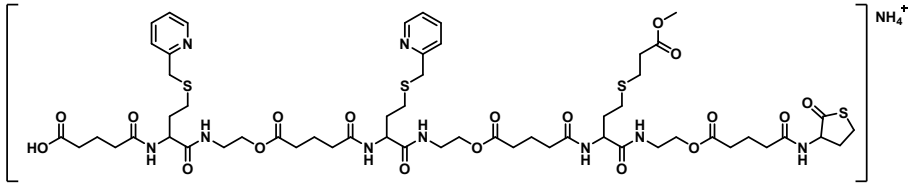	$C_{58}H_{83}N_9O_{18}S_4NH_4$	1339.5154	1339.5077	0.0077	59000
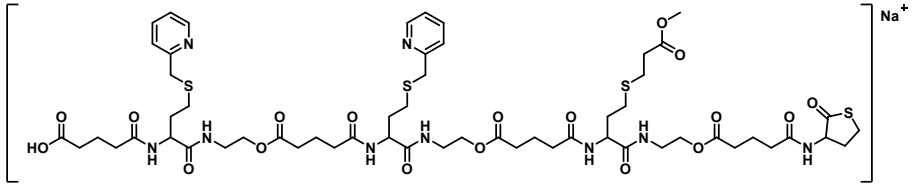	$C_{58}H_{83}N_9O_{18}S4Na$	1344.4628	1344.4632	0.0004	60000
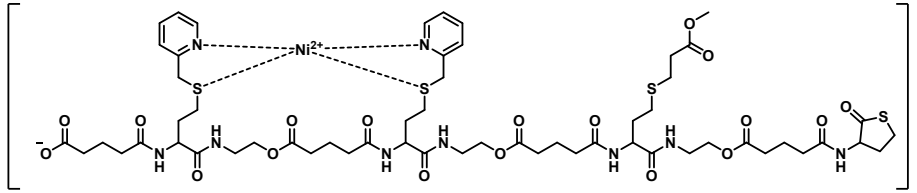	$C_{58}H_{82}N_9NiO_{18}S_4$	1378.4006	1378.4008	0.0002	57000
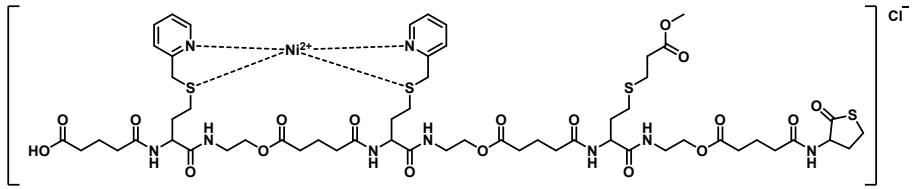	$C_{58}H_{83}ClN_9NiO_{18}S_4$	1414.3773	1414.3775	0.0002	60000

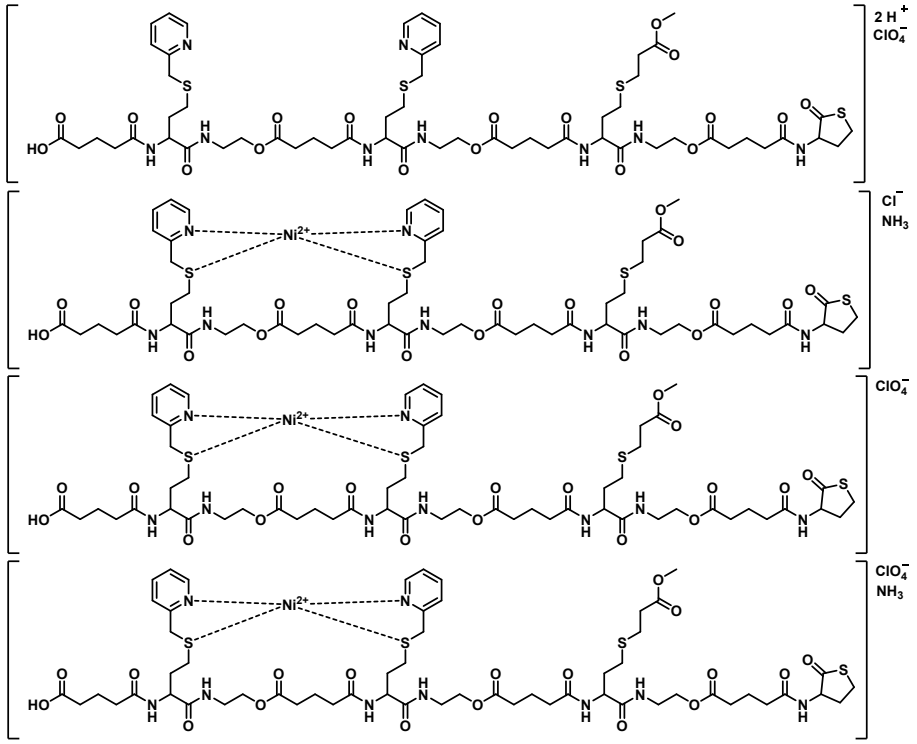

$C_{58}H_{85}ClN_9O_{22}S_4$	1422.4371	1422.4375	0.0004	57000
$C_{58}H_{83}ClN_9NiO_{18}S_4NH_3$	1431.4115	1431.4041	0.0074	58000
$C_{58}H_{83}N_9NiO_{18}S_4ClO_4$	1478.3568	1478.3572	0.0004	57000
$C_{58}H_{83}N_9NiO_{18}S4ClO_4NH_3$	1495.3914	1495.3837	0.0077	54000

Table S13. Peak assignment of S1,2 (Figure S40).

Structure	Sum Formula	m/z (exp)	m/z (theo)	Δm/z	Resolution
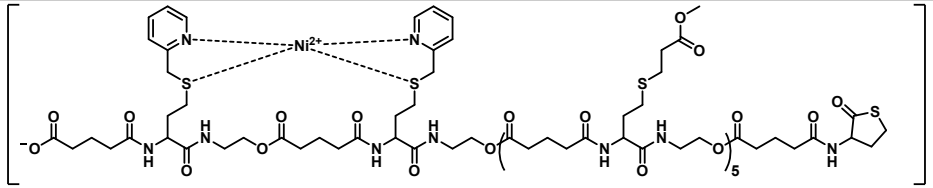	$C_{118}H_{178}N_{17}NiO_{42}S_8$	2818.9743	2818.9429	0.0314	39000
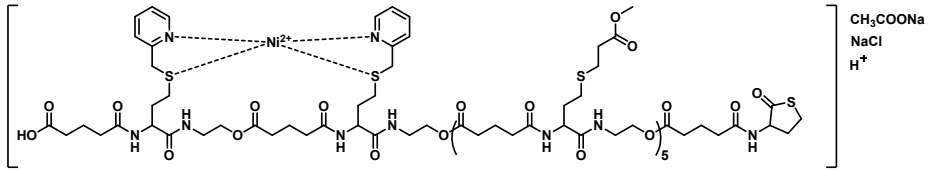	$C_{120}H_{181}ClN_{17}Ni_2O_{44}S_8$	2970.9162	3970.8604	0.0558	36000
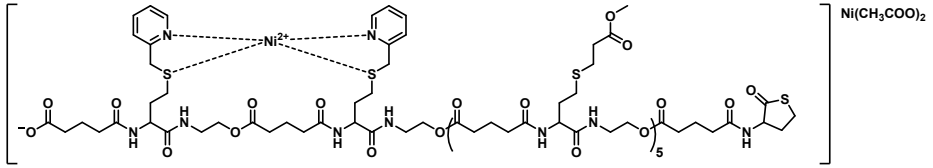	$C_{122}H_{184}N_{17}Ni_2O_{46}S_8$	2994.9393	2994.9048	0.0345	39000
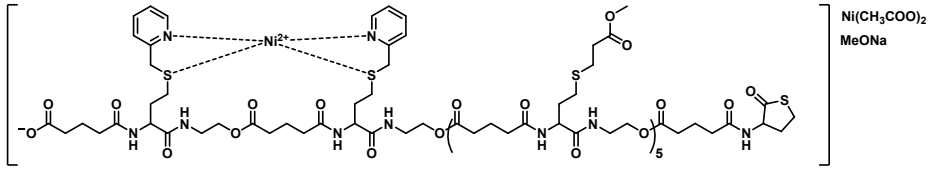	$C_{123}H_{187}N_{17}NaNi_2O_{47}S_8$	3048.9172	3048.9130	0.0042	37000
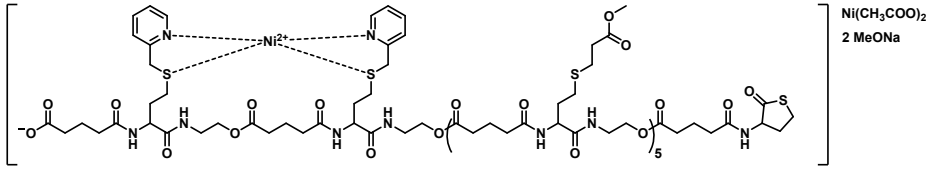	$C_{124}H_{190}N_{17}Na_2Ni_2O_{48}S_8$	3102.8893	3102.9212	0.0319	36000

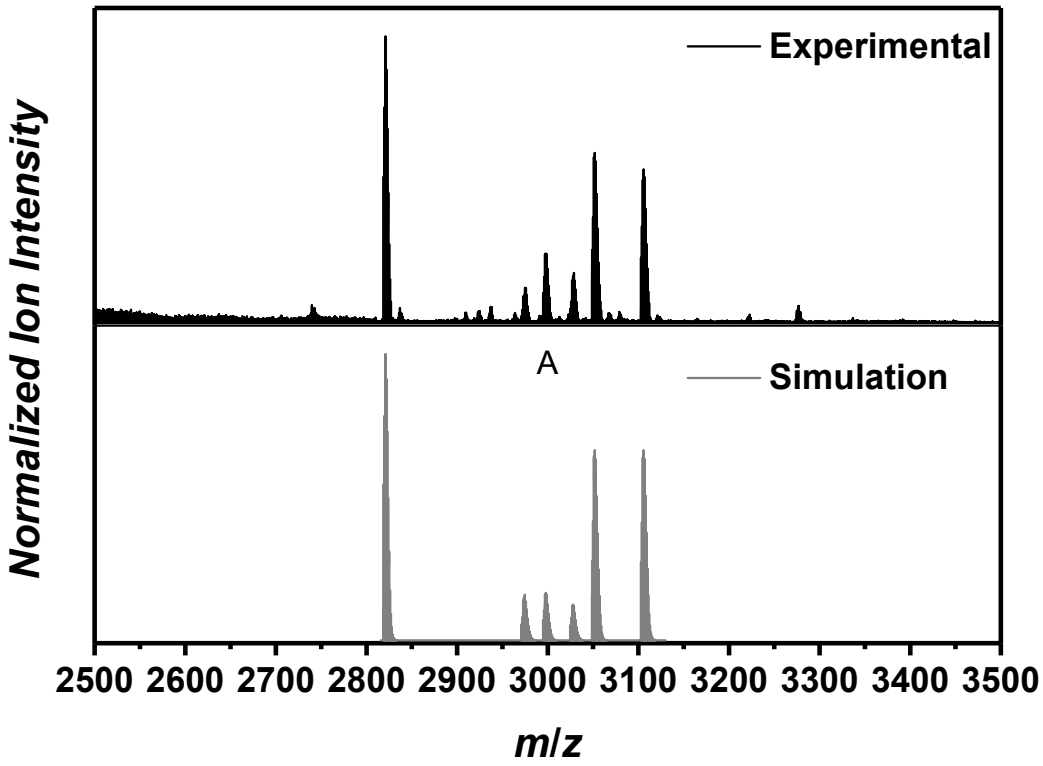

Figure S40. High resolution ESI-MS spectra of the compacted strcuture of S1,2. In Table S13 the assignment of the peaks is displayed.

Molecular Dynamics (MD) simulations

Computational details

All-atom molecular dynamics (MD) simulations were performed using the AMBER 16 package.[5] The heptamers were built by joining nine fragments constructed within Discovery Studio 4.0.[6] The partial atomic charges of each fragment were calculated using the semiempirical AM1-BCC model[7,8] as implemented within the *antechamber* module of AMBER16[9], whereas other force fields parameters are from the 'General AMBER Force Field (GAFF2)'.[10] Following this approach, three heptamers containing the two functional handles separated by 0, 2 and 5 spacer units (S1,2; S1,4 and S1,7 sequences, respectively) were built. The dodecamer and heptadecamer (S1,12 and S1,17 sequences, respectively) were built by joining fourteen and nineteen fragments following the same approach. The structures contain two functional handles separated by 10 and 15 spacer units. To model the coordination of Ni(II) ion with the ligands, Ni(II) ion was placed close to the first functional handle. The ion model for the Ni(II) specie was built using the octahedral dummy atom model reported by Duarte et al.[11] This model consists of six particles, referred as dummy atoms, that are placed around the central Ni(II) ion in an octahedral geometry. Each of the dummy atom carry a charge of +0.5e, while the central Ni(II) ion possesses a charge of -1, for a total net charge of +2. Such charge delocalization away from the metal centre allows for a simplified representation of the partially covalent and partially

electrostatic nature of the coordinative bond, as the space between the metal ion and the ligand is split up into a covalent bond between the metal ion and the positively charged dummy atoms, and an electrostatic interaction between the cationic dummy atoms and the surrounding ligand. The systems were then neutralized with two Cl^- counter ions. To prevent the Ni(II) ion from diffusing too far away from the functional handles, harmonic distance restraints were applied between the central Ni(II) ion and the N and S atoms of the functional handles. Harmonic distance restraints have a half parabolic shape described by a hybrid harmonic-linear function. The function is flat below 2.0 Å (consistent with experimental data for similar ligand structures[12]), beyond which it is parabolic from 2.0 Å to 15.0 Å and becomes linear beyond that. The parabola between 2.0 Å and 15.0 Å is defined by force constants of 25 kcal.mol^{-1}.Å^{-2} for heptamers and 5 kcal.mol^{-1}.Å^{-2} for dodecamer and heptadecamer. The force restraints were chosen to prevent large separation of the Ni(II) ion and the functional handles but allow the Ni(II) ion to diffuse from the functional handles up to a certain distance. Note that such weak restraints still allow considerable backbone fluctuations. The oligomers were then solvated with explicit methanol molecules in a truncated octahedron box with a 10.0 Å buffer in each direction from the solute. The solvated oligomers were relaxed in 4 steps: 1) 10,000 steps of energy minimization of the system consisting in 1,000 steps of steepest descent algorithm, followed by 9,000 cycles of conjugate gradient, with harmonic position restraints on the oligomers (25 kcal.mol^{-1}.Å^{-2}) to allow relaxation of the solvent molecules and the added ions; 2) 10,000 steps of energy minimization of the system consisting in 1,000 steps of steepest descent algorithm, followed by 9,000 cycles of conjugate gradient, with harmonic distance restraints between the Ni(II) ion and the functional handles; 3) heating of the system from 0 to 300 K in 1 ns under constant volume (NVT), with harmonic position restraints placed on the solute (25 kcal.mol^{-1}.Å^{-2}) and with harmonic distance restraints between the Ni(II) ion and the functional handles; 4) equilibration of the system at 300 K for 4 ns under constant pressure (NPT), with harmonic distance restraints between the Ni(II) ion and the functional handles. After these initial relaxation steps, each system was simulated for 750 ns at 300 K under constant pressure (NPT), with harmonic distance restraints between the Ni(II) ion and the functional handles. Periodic boundary conditions were used, and long-range electrostatic interactions were calculated with the Particle-Mesh Ewald (PME) technique with a cut-off of 12.0 Å. The temperature in all simulations was set to 300 K and controlled by the Langevin thermostat with a coupling constant of 1.0 ps and combined with a pseudo-random seed generator.[13] The SHAKE algorithm[14] was employed to constrain bonds involving hydrogen atoms during simulations and an integration time step of 2 fs was used. The resulting trajectories were visualized using the *VMD* software package[15] and snapshots of the MD trajectories were captured using *PyMOL.*[16] Analysis of the trajectories was performed using the *cpptraj* module available in AmberTools.

2D colour-coded distance maps

The complexation of oligomers with nickel ions has been evaluated using 2D colour-coded distance maps. A 2D distance map is a square matrix of order N, where N is the number of fragments in the sequence. Each element (i,j) of the matrix represents the average distance between the centre-of-mass of the ith and jth fragments of the sequence. We used a colour scale to represent the average distances, measured in Angstroms, ranging from the minimum (blue) to the maximum (yellow), as indicated on the vertical bar. The dark blue *diagonal* represents the zero *distance* from a fragment to itself. The 2D difference distance maps are obtained by subtracting the 2D distance map of the non-complexed sequence from that of the complexed sequence.

Root-Mean-Square Fluctuation (RMSF)

To probe how the complexation influences the dynamics of the oligomers, the Root Mean Square Fluctuations (RMSFs) have been evaluated along the sequence of the oligomers. It illustrates the average displacement (i.e. the positional variation *vs.* simulation time) of each fragment, relative to their average structure over the number of atoms in the fragment, thereby giving a measure of the flexibility of a fragment. Higher RMSF values indicate greater flexibility.

It corresponds to the mass-weighted average of atomic fluctuations of each heavy atom for each fragment:

$$RMSF = \sqrt{\frac{1}{T}\sum_{t_j=1}^{N}(x_i(t_j) - \langle x_i \rangle)^2}$$

where T is the duration of the simulation (time steps), $x_i(t_j)$ denotes the position (coordinates) of atom i at time t_j and $\langle x_i \rangle$ is the averaged position of atom i.

Radius of gyration (R_g)

To evaluate the influence of complexation on the overall dimensions of oligomers, the mass-weighted radius of gyration (R_g) of the oligomers has been estimated, giving a measure of the structural compactness. For a polymer chain, it corresponds to the mass-weighted root-mean-square distance of each particle (atom) from its centre-of-mass:

$$R_g = \sqrt{\frac{\sum_{i=1}^{N} m_i (r_i - r_{cm})^2}{\sum_{i=1}^{N} m_i}}$$

where m_i is the mass of atom i, r_i is the position of the atom i and r_{cm} is the position of its centre-of-mass.

Shape descriptors and asphericity parameter

To characterize the shape of the oligomers, the three-dimensional gyration tensor ***T*** of a polymer has been calculated. It corresponds to the arithmetic mean of the second moment of particles along the polymer chain. It can be written as follows:

$$T = \begin{bmatrix} T_{xx} & T_{xy} & T_{xz} \\ T_{yx} & T_{yy} & T_{yz} \\ T_{zx} & T_{zy} & T_{zz} \end{bmatrix}$$

Given that the gyration tensor is a symmetric 3x3 matrix, it can be diagonalized and written in the following form:

$$T = \begin{bmatrix} {\lambda_x}^2 & 0 & 0 \\ 0 & {\lambda_y}^2 & 0 \\ 0 & 0 & {\lambda_z}^2 \end{bmatrix}$$ where the axes of the Cartesian coordinate system are chosen such that the diagonal elements of the matrix (called *principal moments* of the gyration tensor) follow the order: $\lambda_z^2 \geq \lambda_y^2 \geq \lambda_x^2$.

The oligomers shape is characterized by the ratios λ_z/λ_x and λ_y/λ_x of principal moments of gyration tensor, referred to as *shape descriptors*.
The gyration tensor is illustrated in a 2D sketch in Figure S41 for an elongated and a compact polymer, characterized by different and similar eigenvalues ratios, respectively.

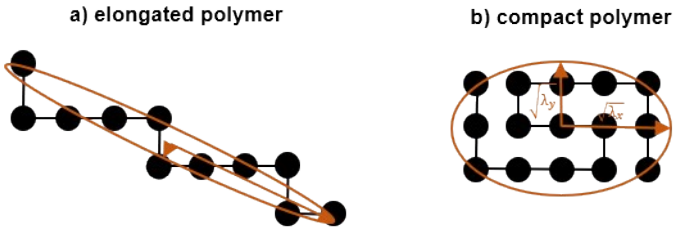

Figure S41. Illustration of the gyration tensor. The gyration ellipsoid is shown for an elongated (a) and a compact polymer (b) conformations in 2D. The ratios of eigenvalues are different for the elongated polymer, indicating strong deviations from a sphere-like shape (adapted from the work of M. Bohn and D. W. Heermann.[17])

The asphericity parameter ***b*** can be defined from the eigenvalues of the gyration tensor. It gives a measure of the deviation from the spherical symmetry and allows to distinguish between spherical and rod-like configurations:

$$b = \lambda_z - \frac{1}{2}(\lambda_x + \lambda_y)$$

with λ_x, λ_y, λ_z corresponding to the eigenvalues of the gyration tensor (λ_z is the largest value).

The asphericity parameter ***b*** is *zero* when the distribution of particles is spherically symmetric and *positive* otherwise.

Solvent accessible surface area (SASA)

To investigate the preference of the structures to lose accessibility (buried) or gain accessibility (exposed) upon complexation, the Solvent-Accessible Surface Area (SASA) was computed using the Linear Combination of Pairwise Overlaps (LCPO)[17] method with a solvent probe radius of 1.7 Å (which approximates the radius of a methanol molecule). This method considers the neighbour list of an atom

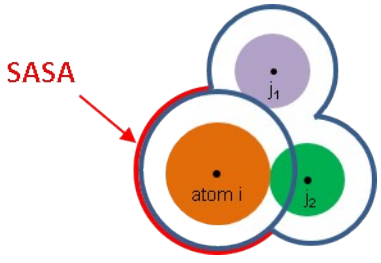

Figure S42. 2D illustration of the LCPO method used for the estimation of the SASA of oligomers. The sphere area of an atom is defined as its van der Waals sphere expanded by the radius of the solvent sphere.

i and subtracts the pairwise overlaps from its isolated sphere area, also considering the overlaps of the neighbours with each other. A 2D sketch of the LCPO method is shown in Figure S42. Higher SASA values indicate more probability of contacts between the surface of oligomers and the solvent molecules.

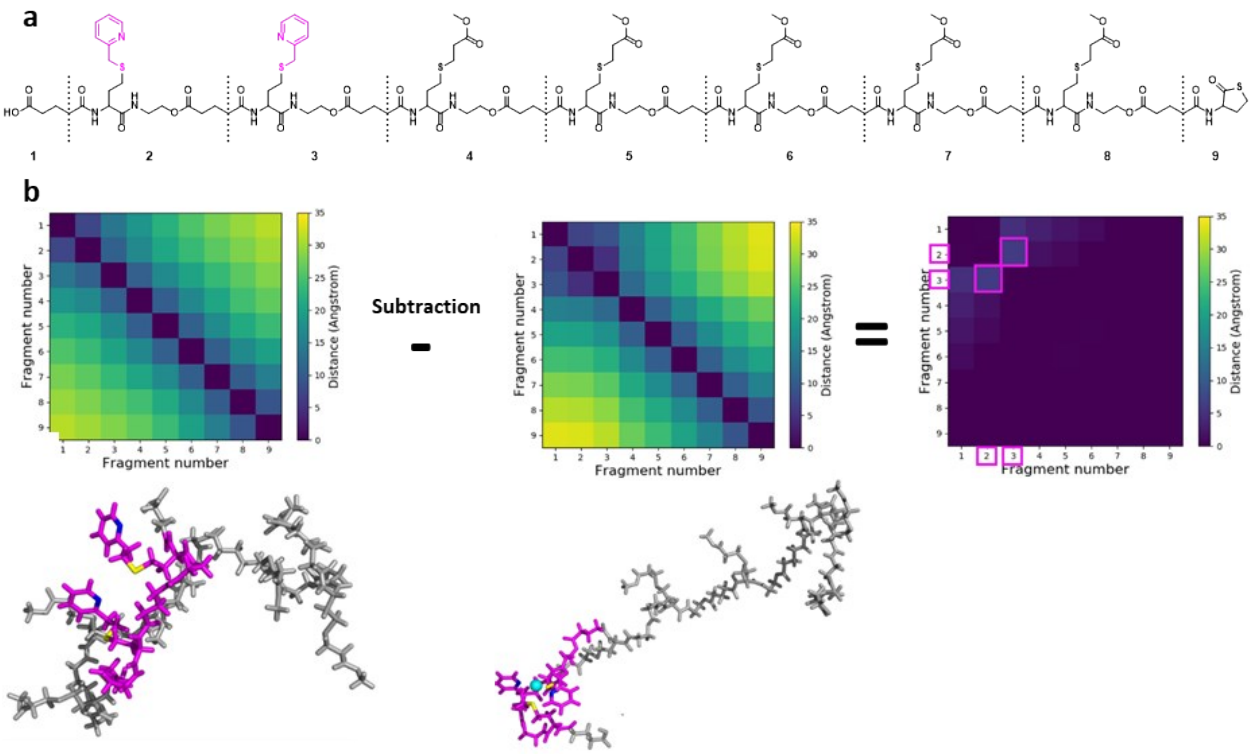

Figure S43. (a) Chemical structure of the model sequence S1,2. Molecular model of the heptamer is constructed by joining nine fragments. The corresponding fragment numbers are also shown. The functional handles are depicted in magenta. **(b) Left:** last snapshots of MD simulations of S1,2 for non-complexed (top) and complexed (bottom) structures, in sticks representation. The two functional handles are shown in magenta, with nitrogen and sulfur atoms in blue and yellow, respectively; the nickel is depicted as a cyan sphere. **(b) Middle:** corresponding 2D distance maps (for the fragment number, see Figure S37a). **(b) Right:** the 2D difference distance map is obtained by subtracting the 2D distance map of the non-complexed sequence from that of the complexed sequence. The regions with large conformational changes, corresponding to complexation sites, are represented by large distances (yellowish regions) and marked with magenta squares.

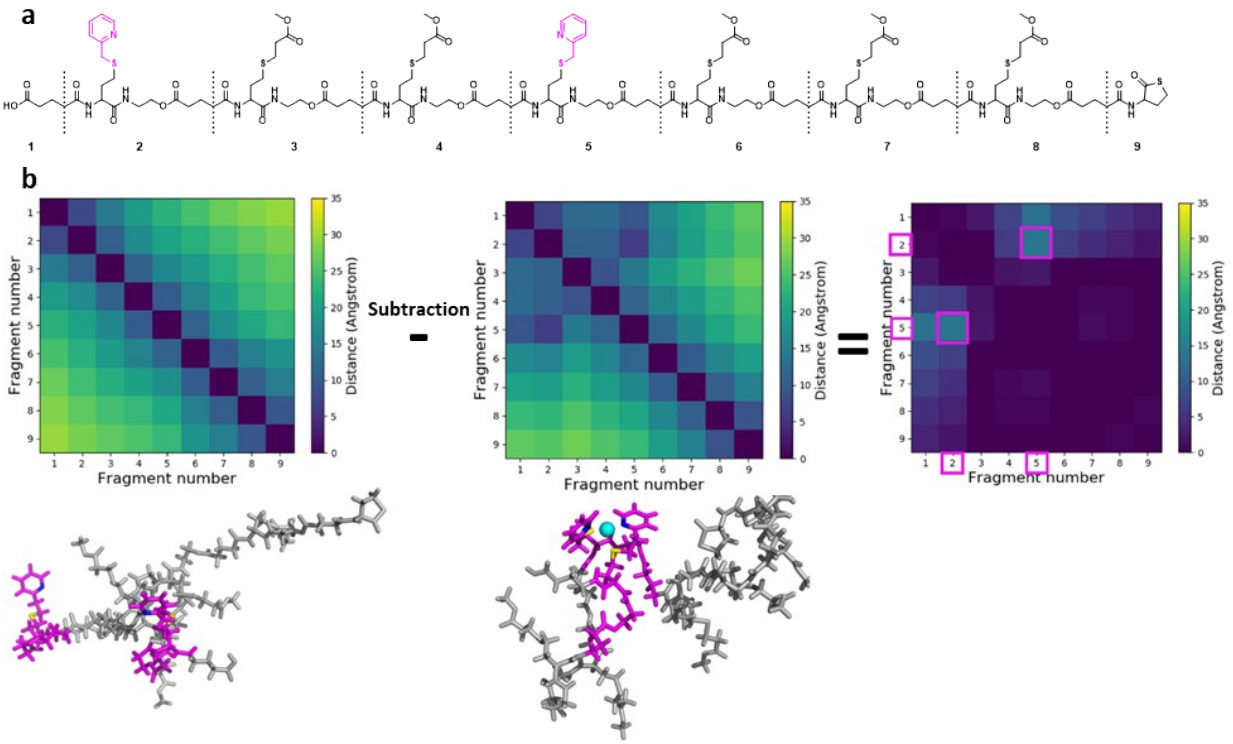

Figure S44. (a) Chemical structure of the model sequence S1,4. Molecular model of the heptamer is constructed by joining nine fragments. The corresponding fragment numbers are also shown. The functional handles are depicted in magenta. **(b) Left:** last snapshots of MD simulations of S1,4 for non-complexed (top) and complexed (bottom) structures, in sticks representation. The two functional handles are shown in magenta, with nitrogen and sulfur atoms in blue and yellow, respectively; the nickel is depicted as a cyan sphere. **(b) Middle:** corresponding 2D distance maps (for the fragment number, see Figure S38a). **(b) Right:** the 2D difference distance map is obtained by subtracting the 2D distance map of the non-complexed sequence from that of the complexed sequence. The regions with large conformational changes, corresponding to complexation sites, are represented by large distances (yellowish regions) and marked with magenta squares.

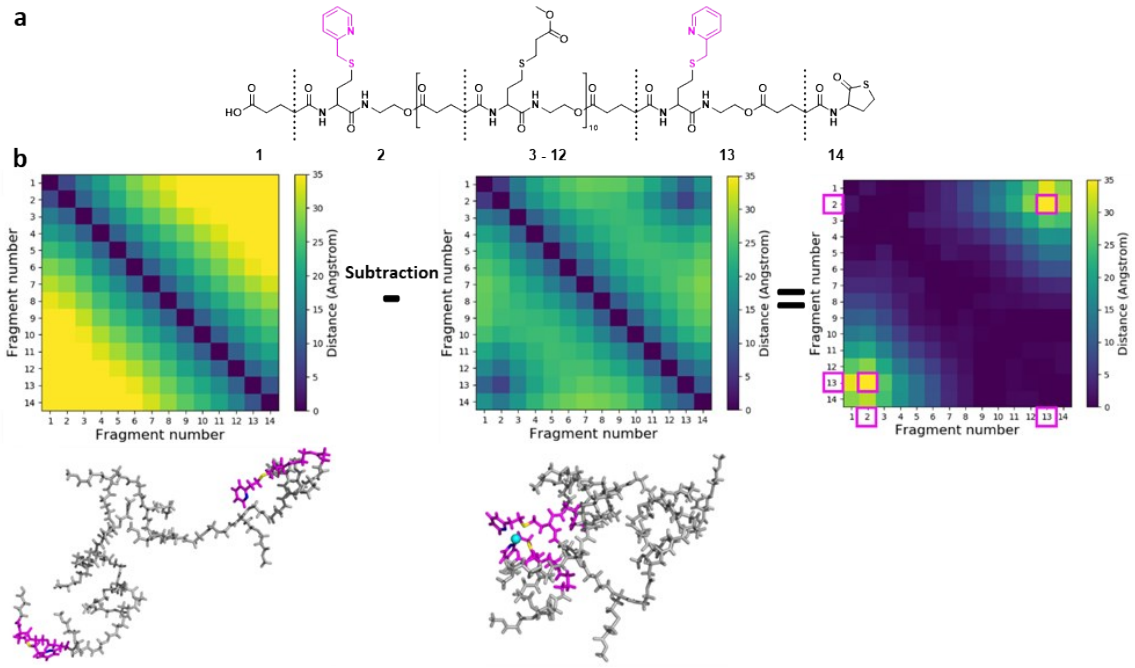

Figure S45. (a) Chemical structure of the model sequence S1,12. Molecular model of the dodecamer is constructed by joining fourteen fragments. The corresponding fragment numbers are also shown. The functional handles are depicted in magenta. **(b) Left:** last snapshots of MD simulations of S1,12 for non-complexed (top) and complexed (bottom) structures, in sticks representation. The two functional handles are shown in magenta, with nitrogen and sulfur atoms in blue and yellow, respectively; the nickel is depicted as a cyan sphere. **(b) Middle:** corresponding 2D distance maps (for the fragment number, see Figure S39a). **(b) Right:** the 2D difference distance map is obtained by subtracting the 2D distance map of the non-complexed sequence from that of the complexed sequence. The regions with large conformational changes, corresponding to complexation sites, are represented by large distances (yellowish regions) and marked with magenta squares.

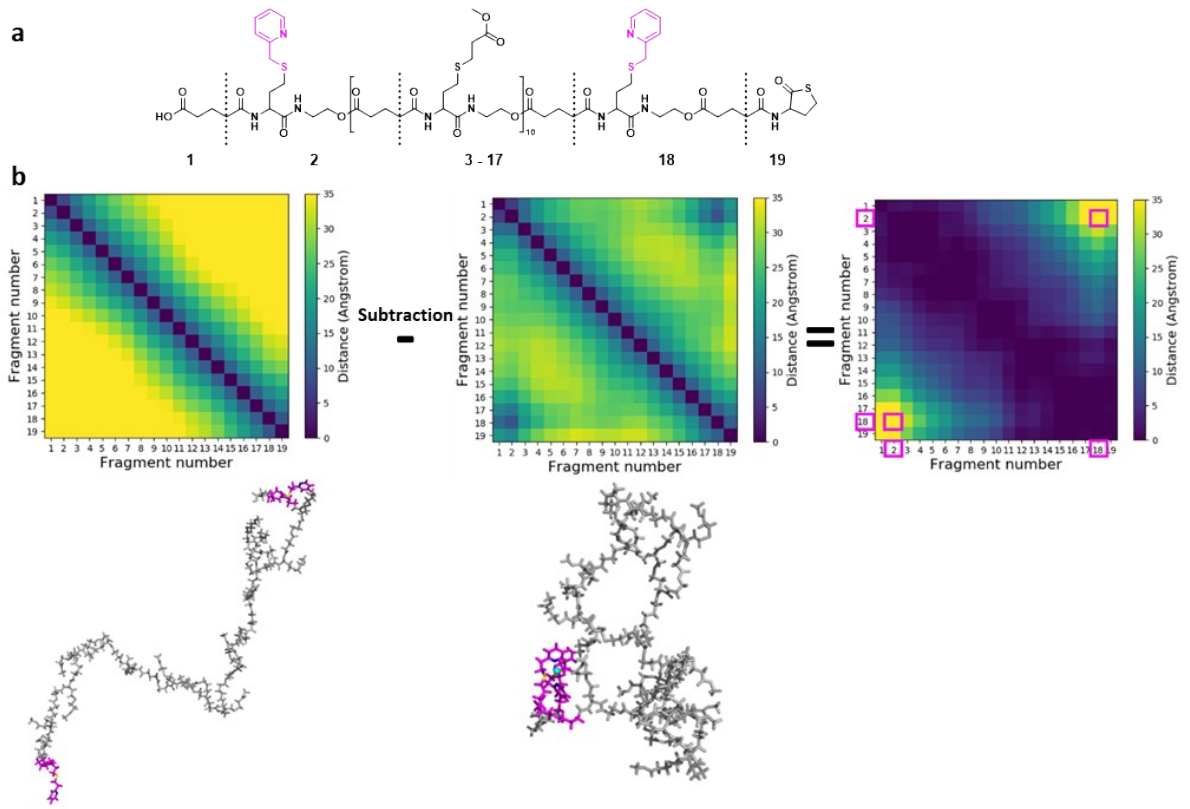

Figure S46. (a) Chemical structure of the model sequence S1,17. Molecular model of the heptadecamer is constructed by joining nineteen fragments. The corresponding fragment numbers are also shown. The functional handles are depicted in magenta. **(b) Left:** last snapshots of MD simulations of S1,17 for non-complexed (top) and complexed (bottom) structures, in sticks representation. The two functional handles are shown in magenta, with nitrogen and sulfur atoms in blue and yellow, respectively; the nickel is depicted as a cyan sphere. **(b) Middle:** corresponding 2D distance maps (for the fragment number, see Figure S40a). **(b) Right:** the 2D difference distance map is obtained by subtracting the 2D distance map of the non-complexed sequence from that of the complexed sequence. The regions with large conformational changes, corresponding to complexation sites, are represented by large distances (yellowish regions) and marked with magenta squares.

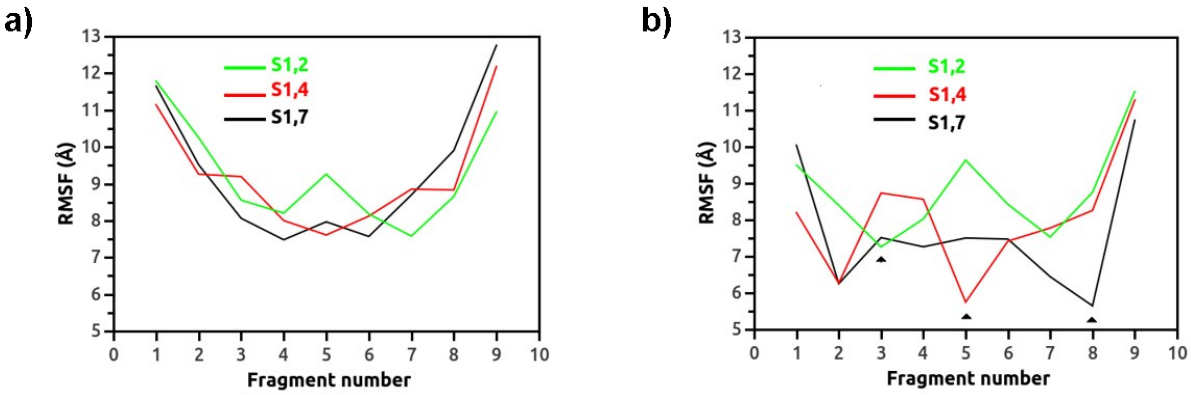

Figure S47. Evolution of the Root Mean Square Fluctuation (RMSF) along the sequence for the non-complexed (a) and complexed (b) heptamers. The minimum RMSF values for the complexed heptamers (b) corresponding to the second functional handles are shown by the arrows.

The profiles of the RMSF versus the fragment number for the non-complexed and complexed heptamers are shown in Figure S43. For the non-complexed heptamers (Figure S47a), the most flexible regions correspond to the termini of the sequences and the most rigid regions are randomly located in the middle of the sequences. Overall, the three non-complexed sequences share similar RMSF distributions. The average RMSF per fragment for the non-complexed S1,2, S1,4 and S1,7 sequences are 9.3, 9.2 and 9.3 Å, respectively. This suggests that the overall flexibility of the non-complexed heptamers is not influenced by the spacer length. On the other hand, for the complexed heptamers (Figure S47b), the RMSF values are slightly lower than those of the non-complexed heptamers. While the termini of the complexed sequences are still the most flexible regions, the functional handles are systematically the most rigid parts. This observation can be explained in terms of binding between the functional handles and the nickel ion that leads directly to the rigidity of the complex. These results suggest that the complexation leads to important conformational changes that influence the flexibility of the heptamers. In contrast with the non-complexed heptamers, the overall flexibility of complexed heptamers decreases as the number of spacer units increases. The average RMSF per fragment for the complexed S1,2, S1,4 and S1,7 sequences are 8.7, 8.1 and 7.4 Å, respectively.

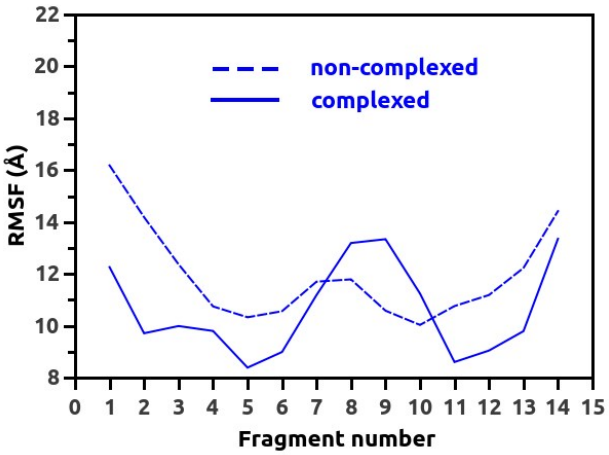

Figure S48. Evolution of the Root Mean Square Fluctuation (RMSF) along the sequence for the non-complexed (a) and complexed (b) dodecamers.

The profiles of the RMSF versus the fragment number for the non-complexed and complexed dodecamers are shown in Figure S48. For the non-complexed dodecamer (dashed line), the most flexible regions correspond to the termini of the sequence and the most rigid regions are randomly located in the middle region of the sequence. The average RMSF per fragment for the non-complexed dodecamer is 11.9 Å. On the other hand, for the complexed dodecamer (solid line), the RMSF values are slightly lower than those of the non-complexed dodecamer. The average RMSF per fragment for the complexed dodecamer decreases to 10.6 Å. While the termini of the complexed sequences are still flexible regions, the complexation with the nickel ion leads to a more structured overall arrangement at the functional handles, but also along the oligomeric chain. The middle part of the sequence corresponds to the most flexible region, as a consequence of the relative extent of local folding of the structure coupled to the complexation.

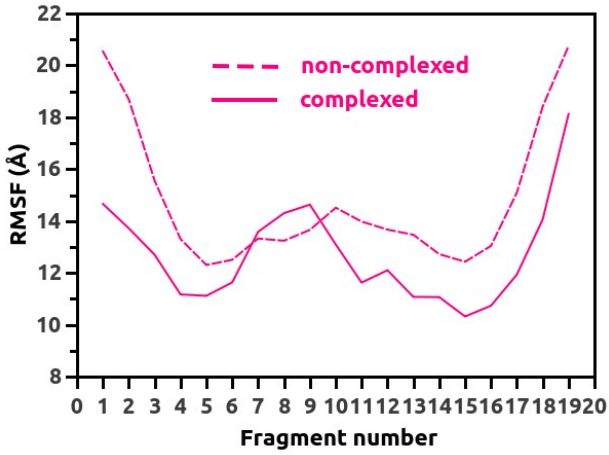

Figure S49. Evolution of the Root Mean Square Fluctuation (RMSF) along the sequence for the non-complexed (a) and complexed (b) heptadecamers.

The profiles of the RMSF versus the fragment number for the non-complexed and complexed heptadecamers are shown in Figure S49. For the non-complexed heptadecamer (dashed line), the most flexible regions correspond to the termini of the sequence and the most rigid regions are randomly

located in the middle region of the sequence. The average RMSF per fragment for the non-complexed heptadecamer is 14.8 Å. On the other hand, for the complexed heptadecamer (solid line), the RMSF values are slightly lower than those of the non-complexed dodecamer. The average RMSF per fragment for the complexed dodecamer decreases to 12.7 Å. While the termini of the complexed sequences are still flexible regions, the complexation with the nickel ion leads to a more structured overall arrangement at the functional handles, but also along the oligomeric chain. The middle part of the sequence corresponds to a highly flexible region, as a consequence of the relative extent of local folding of the structure coupled to the complexation.

Table S14. Statistics on change in compactness of oligomers upon complexation shown as the average Radius of Gyration (Rg) (and their standard deviations) for non-complexed and complexed forms.

Sequences	Average Rg in non-complexed form (Å)	Average Rg in complexed form (Å)
S1,2	15.1 (± 2.7)	15.1 (± 2.5)
S1,4	11.6 (± 2.9)	11.8 (± 2.0)
S1,7	15.0 (± 2.8)	12.5 (± 1.2)
S1,12	19.8 (± 4.0)	14.9 (± 2.8)
S1,17	23.5 (± 4.9)	17.8 (± 2.0)

Table S15. Statistics on change in accessibility of oligomers upon complexation shown as the average Solvent-Accessible Surface Area (SASA) (and their standard deviations) for non-complexed and complexed forms.

Sequences	Average SASA in non-complexed form (Å²)	Average SASA in complexed form (Å²)
S1,2	3072 (± 197)	4275 (± 189)
S1,4	3179 (± 420)	4349 (± 230)
S1,7	3080 (± 269)	4390 (± 238)
S1,12	5191 (± 547)	6778 (± 323)
S1,17	7173 (± 525)	8459 (± 372)

Supplementary references

1 European Patent office, EP 1964838A1, 2008, 10.

2 C. Mertens, M. Soete, M. L. Ślęczkowski, A. R. A. Palmans, E. W. Meijer, N. Badi and F. E. Du Prez, *Polym. Chem.*, 2020, **11**, 4271–4280.

3 P. Espeel, L. L. G. Carrette, K. Bury, S. Capenberghs, J. C. Martins, F. E. Du Prez and A. Madder, *Angew. Chem. Int. Ed.*, 2013, **52**, 13261–13264.

4 S. Martens, J. Van den Begin, A. Madder, F. E. Du Prez and P. Espeel, *J. Am. Chem. Soc.*, 2016, **138**, 14182–14185.

5 D. A. Case, R. M. Betz, D. S. Cerutti, T. E. Cheatham, T. A. Darden, R. E. Duke, T. J. Giese, T. S. Lee, S. Legrand, P. Li, C. Lin, T. Luchko, R. Luo, B. Madek, D. Mermelstein, K. M. Merz, G. Monard, H. Nguyen, H. T. Nguyen, I.

Omelyan, A. Onufriev, D. R. Roe, A. Roitberg, C. Sagui, C. L. Simmerling, J. Swails, R. C. Walker, J. Wang, R. M. Wolf, X. Wu, L. Xiao and P. A. Kollman, 2016.
6 BIOVIA Dassault Systèmes Discovery Studio Visualizer Software 4.0, 2012.
7 A. Jakalian, B. L. Bush, D. B. Jack and C. I. Bayly, *J. Comput. Chem.*, 2000, **21**, 132–146.
8 A. Jakalian, D. B. Jack and C. I. Bayly, *J. Comput. Chem.*, 2002, **23**, 1623–1641.
9 J. Wang, W. Wang, P. A. Kollman and D. A. Case, *J. Mol. Graph. Model.*, 2005, **25**, 1157–1174.
10 J. Wang, R. M. Wolf, J. W. Caldwell, P. A. Kollman and D. A. Case, *J. Comput. Chem.*, 2004, **25**, 1157–1174.
11 F. Duarte, P. Bauer, A. Barrozo, B. A. Amrein, M. Purg, J. Åqvist, S. Caroline and L. Kamerlin, *J. Phys. Chem. B*, 2014, **118**, 4351–4362.
12 D. Hong, Y. Tsukakoshi, H. Kotani, T. Ishizuka, K. Ohkubo, Y. Shiota, K. Yoshizawa, S. Fukuzumi and T. Kojima, *Inorg. Chem.*, 2018, **57**, 7180–7190.
13 D. S. Cerutti, R. Duke, P. L. Freddolino, H. Fan and T. P. Lybrand, *J. Chem. Theory Comput.*, 2008, **4**, 1669–1680.
14 V. Kräutler and W. F. V. A. N. Gunsteren, *J. Comput. Chem.*, 2001, **22**, 501–508.
15 W. Humphrey, A. Dalke and K. Schulten, *J. Mol. Graph.*, 1996, **14**, 33–38.
16 W. L. DeLano, PyMOL Molecular Graphics System Version 1.8.4.0,Schrödinger, LLC.
17 J. Weiser, P. S. Shenkin and W. C. Still, *J. Comput. Chem.*, 1999, **20**, 217–230.